REGGE THEORY AND HIGH ENERGY HADRON-NUCLEUS SCATTERING

By J. H. Weis*

CERN — Geneva

and

Physics Department, University of Washington, Seattle**

(Presented at the XVI Cracow School of Theoretical Physics, Zakopane, May 25 — June 7, 1976)

The application of Regge theory to high energy hadron-nucleus scattering is reviewed. The usual formalism for scattering off non-relativistic nucleons in a nucleus is applied to obtain momentum space expressions for multiple Regge exchange contributions. These expressions are analyzed in some detail and applied to obtain the total and single particle inclusive cross-sections. Using hadron-hadron scattering phenomenology as an input we discuss hadron-nucleus scattering phenomenology for current energies ($p_{lab} \lesssim 10^4$ GeV/c) and available nuclei ($A \lesssim 250$). The applications discussed here are only the simplest ones; hadron-nucleus scattering should allow many other tests of the theory not possible in hadron--hadron scattering. The Reggeon calculus approach taken here is more convenient for explicit calculations but less intuitive than parallel discussions based on the space-time picture in the multiperipheral model or on the parton model. The latter are discussed briefly in an Appendix.

1. Introduction

In these lectures I will review the application of Regge theory to high-energy hadron--nucleus interactions. The Regge model (with its close relative, the multiperipheral model) provides a very compact framework for understanding the basic features of high-energy hadron-hadron interactions. It also has a firm theoretical grounding since it satisfies the requirements of analyticity and both direct (s)-channel and crossed (t)-channel unitarity (and in the case of the multiperipheral model has a foundation in "soft" field theory). For these two reasons it seems very important to know if it can also give a successful description of hadron-nucleus collisions where different time scales are involved.

---

* A P. Sloan Foundation Fellow. Work supported in part by U. S. Energy Research and Development Administration.

** Address: Physics Department, University of Washington, Seattle, WA 98105, USA.

The theoretical tightness of the model is one of its most attractive features. In principle, hadron-nucleus scattering is determined by the Regge model for hadron-hadron scattering and some knowledge of nuclear structure. Therefore, a knowledge of hadron-hadron Regge phenomenology should enable us to understand completely hadron-nucleus scattering. If this is not the case we shall be in a quandary since the model is the only available one in which full satisfaction of analyticity and unitarity is built in from the start.

The qualitative predictions of the Regge model for hadron-nucleus scattering are not too difficult to obtain (particularly for asymptotic energies). We shall see in Section 5 that they are not manifestly inconsistent with present data. However, we are now reaching a stage of greatly increased experimental knowledge (particularly at finite energies) and more detailed calculations with the model are in order. I hope this review will be of some use to people who wish to confront the model with the data. Real calculations often involve a certain amount of technical details as is often the case with a rather complete model. While this can make life difficult for us, it should not be allowed to detract from the attractiveness of the model from a theoretical point of view.

In Section 2, a general multiple scattering formalism is developed. This is used as the basis for Section 3, where the double scattering diagram is studied in detail in the Regge model. In Section 4, multiparticle production is discussed. Then in Section 5 we make use of our knowledge of hadron-hadron phenomenology to discuss the general phenomenological implications of the Regge model for hadron-nucleus collisions at current energies ($p_{\text{lab}} \lesssim 10^4$ GeV/c) and available nuclei ($A \leqslant 250$).

In the Appendix we study the space-time picture of collisions in the multiperipheral model which is the prototype of models with Regge behaviour. This gives a simple intuitive picture for a number of the results discussed in the main text.

We conclude this introduction with a review of the Regge model for elastic hadron--hadron scattering. We then introduce the application of the model to hadron-nucleus scattering by discussing qualitatively the elastic scattering of an incident hadron on the various nucleons in a nucleus as it passes through it. Although this example will be seen to be totally unrealistic, it will serve to introduce some ideas used later.

1.1. Regge model for hadron-hadron elastic scattering

For hadron-hadron elastic scattering the Regge-pole exchange amplitude [1] is given by (Fig. 1)

$$\mathscr{A}_{h_1h_2}(s, t) \sim \beta_{h_1}(t)\tilde{\xi}s^{\alpha(t)}\beta_{h_2}(t). \tag{1.1}$$

$$\tilde{\xi} = \frac{e^{-i\pi\alpha(t)} + \tau}{-\sin \pi\alpha(t)} \tag{1.2}$$

and $\tau = \pm 1$ is the signature. We will be discussing high-energy scattering so usually the Regge trajectory will be taken to be the Pomeron with

$$\alpha_P(t) = \alpha_P(0) + \alpha'_P(t) \approx 1 + \tfrac{1}{4}t. \tag{1.3}$$

In the "laboratory frame",

$$p_{h_1} = (p_{h_1 0}, 0, 0, p_{h_1 z}),$$

$$p_{h_2} = (m_2, 0, 0, 0),$$

$$p'_{h_1} = (p'_{h_1 0}, q_x, q_y, p'_{h_1 z}), \tag{1.4}$$

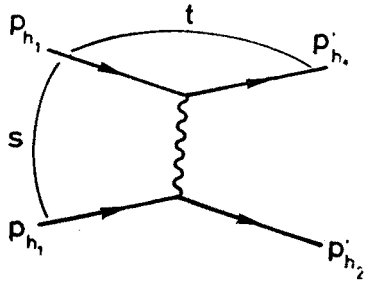

Fig. 1. The elastic hadron-hadron Regge exchange amplitude

we have

$$s = (p_{h_1} + p_{h_2})^2 = 2m_2 p_{h_1 0} + m_1^2 + m_2^2,$$

$$t = (p_{h_1} - p'_{h_1})^2 = (p_{h_1 0} - p'_{h_1 0})^2 - q_T^2 - (p_{h_1 z} - p'_{h_1 z})^2 = -q_T^2 + O\left(\frac{1}{s}\right). \tag{1.5}$$

The invariant momentum transfer can thus be expressed solely in terms of the transverse momentum transfer $\vec{q}_T = (q_x, q_y)$. Using (1.5) we can rewrite (1.1) as

$$\mathscr{A}_{h_1 h_2}(s, t) \sim i\beta_{h_1}(0)\beta_{h_2}(0) s^{\alpha(0)} e^{-(\gamma_1 + \gamma_2 + \alpha' \ln s) q_T^2}, \tag{1.6}$$

where we have parametrized the Regge residues as

$$\beta_{h_i}(t) = \beta_{h_i}(0) e^{\gamma_i t} \tag{1.7}$$

and neglected the t dependence of ξ which gives a small t-dependent phase.

An interesting physical picture for scattering by Regge exchange can be obtained if we consider the Fourier transform of Eq. (1.6) in the variable $\vec{q}_T$

$$\tilde{\mathscr{A}}_{h_1 h_2}(s, \tilde{b}) \equiv \frac{1}{2\pi} \int d^2 q_T e^{-i\vec{b} \cdot \vec{q}_T} \mathscr{A}_{h_1 h_2}(s, -q_T^2)$$

$$\sim \frac{i\beta_{h_1}(0)\beta_{h_2}(0) s^{\alpha(0)}}{2(\gamma_1 + \gamma_2 + \alpha' \ln s)} \exp\left(\frac{-b^2}{4(\gamma_1 + \gamma_2 + \alpha' \ln s)}\right). \tag{1.8}$$

The quantity $\vec{b}$ is the impact parameter of the collision. We can interpret (1.8) by saying that the incident hadron sees the hadron at rest as an object with a Gaussian matter

density of width $2\sqrt{\gamma_1+\gamma_2+\alpha' \ln s}$. Its size thus increases with energy. However, the density decreases as $(\gamma_1+\gamma_2+\alpha' \ln s)^{-1}$ as the energy increases. We can thus picture the hadron as shown in Fig. 2. As a check of this we note that

$$s\sigma_{hh'}^{tot} \sim \text{Im}\, \mathscr{A}(s, 0) \propto s^{\alpha(0)}$$

$$\propto \zeta(\pi R^2) \propto \left(\frac{s^{\alpha(0)}}{\ln s}\right)(\sqrt{\ln s})^2 \propto s^{\alpha(0)}.$$

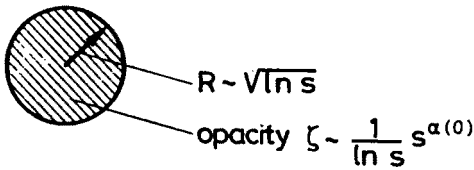

Fig. 2. Front view of a hadron

1.2. Elastic rescattering

As an application of the above simple Regge-pole model, we consider the elastic rescattering of an incident hadron as it passes through a nucleus. Since we are discussing high-energy scattering and nuclear binding energies are small, we expect that we can treat the nucleus as a collection of A independent nucleons. Thus as a naïve first guess we might expect that

$$\sigma_{hA} \approx A\sigma_{hN} \propto R^3 s^{\alpha(0)-1}, \tag{1.9}$$

where R now is the nuclear radius and the last step follows from the approximate constancy of nuclear densities. In other words, we would have

$$\beta_A = A\beta_N \tag{1.10}$$

where β_N in the Pomeron coupling to a nucleon

$$\beta_N = \beta_p = \beta_n.$$

However, this totally neglects the facts that the nucleons have a finite size and that the nucleons at the front side of the nucleus screen those deeper in [2]. To discuss this effect we need to distinguish two cases [3].

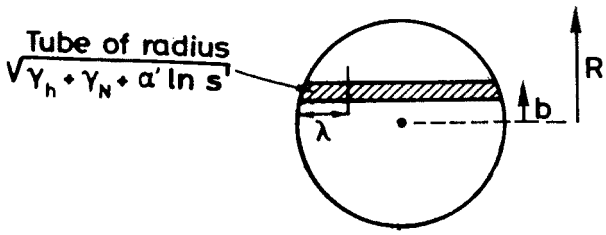

Fig. 3. Side view of nucleus ($\sqrt{\alpha' \ln s} \ll R$)

(*i*) $\sqrt{\gamma_h+\gamma_N+\alpha' \ln s} \ll R$. In this case the nucleons are much smaller than the nucleus. We can picture the process as shown in Fig. 3. The incident hadron at impact parameter $\vec{b}$ interacts with nucleons whose centres are within a tube of radius $\sqrt{\gamma_h+\gamma_N+\alpha' \ln s}$, since in each collision it is scattered through only a very small angle[1]. It can interact therefore only with those nucleons within a mean free path λ of the front. Therefore, we have

$$\sigma_{hA} \propto \frac{\lambda R^2}{R^3} A\sigma_{hN} \propto R^2 \quad \text{(Regime (i))}. \tag{1.11}$$

(*ii*) $\sqrt{\gamma_h+\gamma_N+\alpha' \ln s} \gg R$. Now each nucleon as seen by the incident hadron appears much larger than the nucleus (see Fig. 4). On the other hand, due to Eq. (1.8), they are

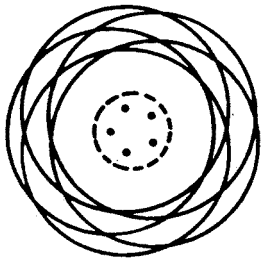

Fig. 4. Front view of nucleus ($\sqrt{\alpha' \ln s} \gg R$)

also very transparent. Thus the nucleus appears to be a collection of very large and diffuse overlapping disks. Because of the transparency, there is now little screening and

$$\sigma_{hA} \sim A\sigma_{hN} \propto R^3 \quad \text{(Regime (ii))}. \tag{1.12}$$

This last result is disturbing since one would expect that at least for large nuclei we would have a geometrical cross-section $\sigma_{hA} \propto R^2$. We first note that for accelerator energies we will never be in regime (*ii*). We have

$$\gamma_p \approx 1.7 \text{ GeV}^{-2}, \quad \alpha' \approx 0.25 \text{ GeV}^{-2}, \quad \ln s \approx 8 \text{ (at ISR)}, \tag{1.13}$$

so

$$\sqrt{2\gamma_N+\alpha' \ln s} \approx \sqrt{5 \text{ GeV}^{-2}} \approx 2 \text{ GeV}^{-1}$$

while

$$R = R_0 A^{1/3} \approx 1 \text{ fm } A^{1/3} \approx 5 \text{ GeV}^{-1} A^{1/3}. \tag{1.14}$$

More importantly, there is good reason that we should not believe the conclusion (1.12). Let us consider the elastic cross-section

$$\sigma^{el}_{h_1h_2} \sim \frac{1}{16\pi} \frac{1}{s^2} \int dq_T^2 |\mathscr{A}_{h_1h_2}(s, -q_T^2)|^2 \propto \frac{s^{2(\alpha(0)-1)}}{\gamma_1+\gamma_2+\alpha' \ln s} \tag{1.15}$$

[1] We have $|\vec{q}_T| \sim 1/\sqrt{\ln s}$ and $p_{hz} \sim s$, so $\tan\theta \approx |\vec{q}_T|/|p_{hz}|$ is very small for large s.

and so in regime (*ii*)

$$\sigma^{\mathrm{el}}_{h_1h_2} \ll \sigma^{\mathrm{tot}}_{h_1h_2}, \quad \text{or} \quad \sigma^{\mathrm{el}}_{h_1h_2} \ll \sigma^{\mathrm{inel}}_{h_1h_2}. \tag{1.16}$$

Therefore inelastic processes must be very important in this regime and rescattering of the produced particles must also be taken into account. This will be one of the main goals of our study.

We shall find [4, 5] that inelastic processes become important at energies on the order of

$$p_{hz} \approx R\mu^2, \tag{1.17}$$

where μ^2 is a typical hadronic mass. This is well within regime (*i*) so Eq. (1.11) is not generally valid. In the remainder of this work we shall obtain the correct behaviour of the total cross-section and other interesting quantities in regime (*i*). We shall not return to régime (*ii*), since it is not experimentally accessible at present.

In our discussion of inelastic processes we will make frequent reference to the multiperipheral model which is the prototype of models which produce Regge poles. A typical inelastic process is shown in Fig. 5a. The chief characteristic of the model is that the momentum transfers t_i are limited. These production processes then lead to Regge behaviour of the elastic amplitude as shown in Fig. 5b. The model is discussed further in the Appendix, but for a complete treatment we refer the reader to the excellent review article of Baker and Ter-Martirosyan [6].

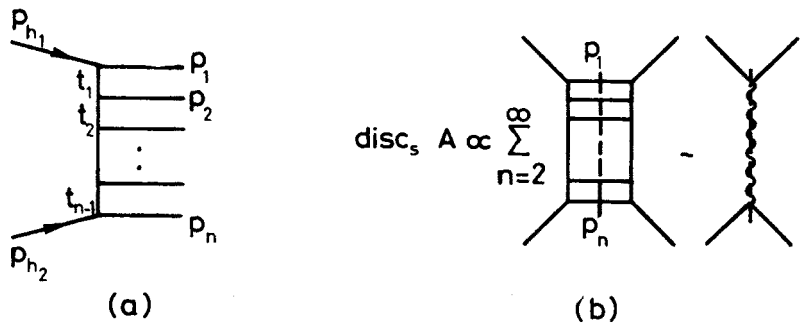

Fig. 5. a) Multiperipheral production process, b) generation of Regge pole through unitarity in multiperipheral model

2. *Multiple scattering formalism*

Before turning to the study of inelastic processes, we wish to develop the rescattering phenomenon in a more formal manner. This formalism will serve as a basis for our later work. We represent a scattering from a single nucleon via Regge exchange by Fig. 6a. Similarly, a multiple *elastic* scattering from n different nucleons is represented by Fig. 6b. The full amplitude is a sum over all such diagrams,

$$\mathscr{A}_{hA} = \sum_{n=1}^{A} \mathscr{A}^{(n)}_{hA}. \tag{2.1}$$

We shall regard diagrams such as those in Fig. 6 as Feynman diagrams where the Regge exchange is given by (1.1). By including all possible diagrams we will be assured of obtaining amplitudes which satisfy the contraints of unitarity.

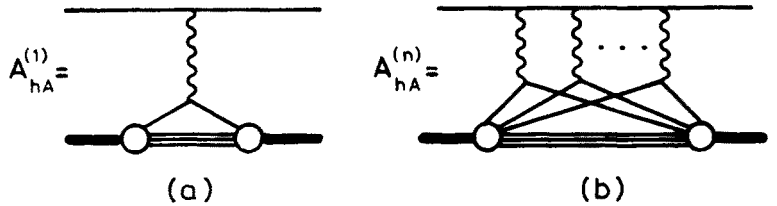

Fig. 6. Multiple elastic rescattering diagrams. The heavy line represents the nucleus A and light lines represent hadrons

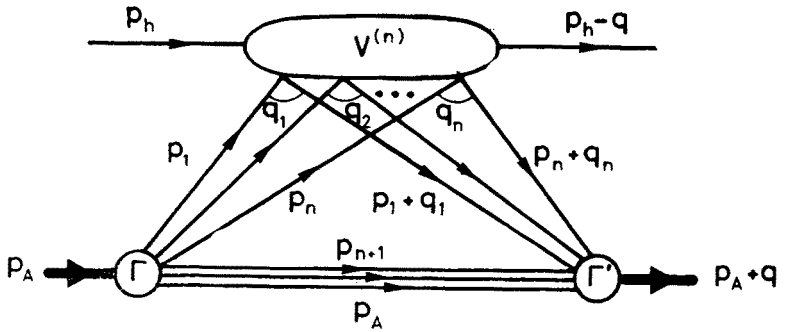

Fig. 7. General n-fold rescattering diagram

Let us consider a general n-fold scattering (see Fig. 7) of which Fig. 6b is a special case [7, 8]. Following the conventions of Bjorken and Drell [9] we have[2]

$$i\mathscr{A}^{(n)} = \frac{1}{A!}\prod_{i=1}^{A}\int\frac{d^4p_i}{(2\pi)^4}\prod_{i=1}^{n}\frac{d^4q_i}{(2\pi)^4}(2\pi)^4\delta^4\left(p_A-\sum_{i=1}^{A}p_i\right)(2\pi)^4$$

$$\times\,\delta^4\left(p_A+q-\sum_{i=1}^{A}p_i-\sum_{i=1}^{n}q_i\right)\frac{A!}{(A-n)!n!}$$

$$\times\,\frac{(iV^{(n)})\,(i\Gamma)\,(i\Gamma')}{\prod_{i=1}^{A}(-i(p_i^2-m^2+i\varepsilon))\prod_{i=1}^{n}(-i((p_i+q_i)^2-m^2+i\varepsilon))}\,, \tag{2,2}$$

where the combinatorial factors arise from the different ways of choosing the n nucleons.

It is convenient to introduce momenta k_i defined by

$$p_i = \frac{p_A}{A}+k_i. \tag{2.3}$$

[2] $S \equiv 1+i(2\pi)^4\,\delta^4(\Sigma p_i)\,\mathscr{A}$.

We shall always work in the "laboratory frame" where the nucleus is at rest

$$p_A = (M, 0, 0, 0),$$

$$p_h = (p_{h0}, 0, 0, p_{hz}) \sim (p, 0, 0, p), \tag{2.4}$$

where

$$M \equiv A(m-\mathscr{E}) \tag{2.5}$$

with $m = m_N$ and $\mathscr{E}$ the binding energy per nucleon. The propagators in (2.2) then become

$$p_i^2 - m^2 = -\Delta^2 + 2\frac{p_A}{A}k_i + k_i^2 \approx -\Delta^2 + 2mk_{i0} - \vec{k}_i^2$$

and

$$(p_i+q_i)^2 - m^2 \approx -\Delta^2 + 2m(k_{0i}+q_{i0}) - (\vec{k}_i+\vec{q}_i)^2, \tag{2.6}$$

where

$$\Delta^2 = m^2 - (m-\mathscr{E})^2 \approx 2m\mathscr{E}$$

and in the final forms we have treated the nucleons as non-relativistic,

$$k_{i0} \ll k_{iz} \ll m, \quad q_{i0} \ll q_{iz} \ll m, \quad \mathscr{E} \ll m. \tag{2.7}$$

We expect the vertices Γ to be large only in this regime. The amplitude $V^{(n)}$ depends on variables such as[3]

$$s_i \equiv (p_h+p_i)^2 = m_h^2 + m^2 - \Delta^2 + 2mp + 2k_i\left(p_h + \frac{p_A}{A}\right) + k_i^2 \sim 2mp \equiv s^* \tag{2.8}$$

and

$$\tilde{M}_i^2 \equiv (p_h - q_i)^2 = m_h^2 + q_i^2 - 2p(q_{i0} - q_{iz}) \approx m_h^2 - q_i^2 + 2pq_{iz}. \tag{2.9}$$

We now suppose that all the important singularities in the virtual nucleon masses $[p_i^2, (p_i+q_i)^2]$ reside in the explicit propagators in (2.2). This, along with (2.7) means that we are essentially treating the nucleus as a collection of precisely A non-relativistic nucleons. We see from (2.8) and (2.9) that $V^{(n)}$ then does not have any significant dependence on k_{i0} and q_{i0}. The integrals over these variables can thus be done explicitly.

We first consider the q_{i0} integrals. Each propagator has a singularity in the lower half plane

$$q_{i0} = -k_{i0} + \frac{\Delta^2 + (\vec{k}_i+\vec{q}_i)^2 - i\varepsilon}{2m}. \tag{2.10}$$

---

[3] The energies $s_i \sim s^*$ are those available for particle production in the model. Terms of order pk_{i0} are neglected in the last step. This neglect of Fermi motion is reasonable at high energies where there is no rapid variation of $V^{(n)}$ in s_i.

We can use the momentum conservation constraints

$$\sum_{i=1}^{n} q_i = 0, \quad \sum_{i=1}^{A} k_i = 0 \tag{2.11}$$

to do, say, the q_{n0} integral, which gives rise to a denominator

$$(p_n+q_n)^2-m^2+i\varepsilon \approx -\Delta^2+2m(k_{n0}+q_0-\sum_{i=1}^{n-1} q_{i0})-(\vec{k}_n+\vec{q}_n)^2 \tag{2.12}$$

which has singularities in the upper half q_{i0} plane

$$q_{i0} = k_{n0}+q_0-\sum_{\substack{k=0\\k\neq i}}^{n-1} q_{k0}-\frac{\Delta^2+(\vec{k}_n+\vec{q}_n)^2-i\varepsilon}{2m}. \tag{2.13}$$

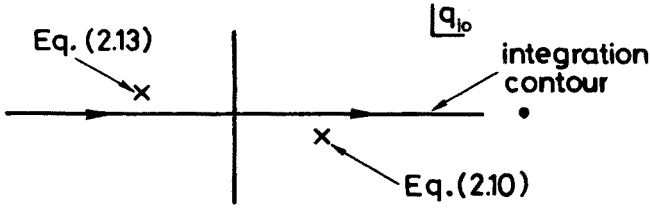

Fig. 8. The q_{i0} complex plane

The situation in the q_{i0} plane is then as shown in Fig. 8. We perform each q_{i0} integral by closing the contour in the lower half plane encircling the pole of (2.10). Each propagator gives

$$\frac{i}{((p_i+q_i)^2-m^2+i\varepsilon)} \to \frac{2\pi}{2m}\bigg|_{q_{i0}=-k_{i0}+\frac{\Delta^2+(\vec{k}_i+\vec{q}_i)^2}{2m}} \tag{2.14}$$

or $i = 1, 2, \ldots, n-1$, and

$$\prod_{i=1}^{n}\left(\frac{i}{(p_i+q_i)^2-m^2+i\varepsilon}\right) \to \left(\frac{2\pi}{2m}\right)^{n-1} \frac{i}{-n\Delta^2-2m\sum_{i=n-1}^{A} k_{i0}-\sum_{i=1}^{n}(\vec{k}_i+\vec{q}_i)^2}. \tag{2.15}$$

The k_{i0} integrals can be done in a similar manner using (2.11) to eliminate k_{n0}. Each variable k_{i0} ($i \neq n$) has one pole in the lower half plane (from $p_i^2-m^2+i\varepsilon$) and in the upper half plane either one pole (for $i = 1, \ldots, n-1$ arising from $p_n^2-m^2+i\varepsilon$) or two poles (for $i = n+1, \ldots, A$ arising from $p_n^2-m^2+i\varepsilon$ and Eq. (2.15)). Closing each contour below gives

$$\prod_{i=1}^{A}\left(\frac{i}{p_i^2-m^2+i\varepsilon}\right) \to \left(\frac{2\pi}{2m}\right)^{A-1} \frac{i}{-A\Delta^2-\sum_{i=1}^{A}\vec{k}_i^2}. \tag{2.16}$$

Substituting (2.16) and (2.15) (with the $k^i{}_0$ taking on their given values) into (2.2) we have

$$\mathscr{A}^{(n)} = \frac{1}{(A-n)!n!} \prod_{\substack{i=1 \\ i\neq n}}^{A} \int \frac{d^3k_i}{(2\pi)^3 2m} \prod_{i=1}^{n-1} \int \frac{d^3q_i}{(2\pi)^3 2m} V^{(n)}$$

$$\times \left(\frac{\Gamma}{A\Delta^2 + \sum_{i=1}^{A} \vec{k}_i^2} \right) \left(\frac{\Gamma'}{A\Delta^2 + \sum_{i=1}^{A} (\vec{k}_i + \vec{q}_i)^2} \right), \tag{2.17}$$

where $\vec{q}_i \equiv 0$ for $i > n$ and (2.11) is implicit. We see that doing the energy integrals has put all but two of the nucleons on mass shell.

The last two factors in (2.17) can be identified with the non-relativistic wave function of the nucleus. To see this we imagine maesuring the locations of the A nucleons using

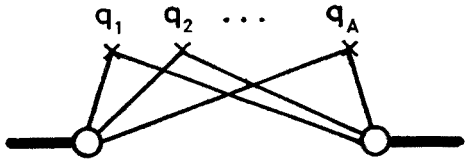

Fig. 9. Hypothetical scattering process

a weak probe. In momentum space this corresponds to the process in Fig. 9. The amplitude in terms of the non-relativistic wave function is given by

$$A! \prod_{i=1}^{A-1} \int \frac{d^3p_i}{(2\pi)^3} \psi(p_i)\psi^*(p_i + q_i), \tag{2.18}$$

where

$$\sum_{i=1}^{A} q_i = 0.$$

This process can also be calculated using the relativistic formulation of (2.2)

$$\prod_{i=1}^{A} \int \frac{d^4p_i}{(2\pi)^4} (2\pi)^4 \delta^4 \left(p_A - \sum_{i=1}^{A} p_i \right) \frac{(i\Gamma)(i\Gamma')}{\prod_{i=1}^{A} (-i(p_i^2 - m^2 + i\varepsilon))(-i((p_i+q_i)^2 - m^2 + i\varepsilon))}.$$

Following the same steps which led to (2.17) we obtain

$$\prod_{i=1}^{A-1} \int \frac{d^3k_i}{(2\pi)^3 (2m)} \left(\frac{\Gamma}{A\Delta^2 + \sum_{i=1}^{A} \vec{k}_i^2} \right) \left(\frac{\Gamma'}{A\Delta^2 + \sum_{i=1}^{A} (\vec{k}_i + \vec{q}_i)^2} \right). \tag{2.19}$$

Inserting the Fourier transforms[4]

$$\psi(p_i) = \prod_{i=1}^{A} \int d^3x_i e^{-i\vec{p}_i \cdot \vec{x}_i} \psi(x_i) \delta^3\Big(\sum_{i=1}^{A} x_i\Big)$$

in (2.18) and comparing with (2.19) gives

$$\frac{\Gamma}{A\Delta^2 + \sum_{i=1}^{A} \vec{k}_i^2} = \sqrt{(2m)^{A-1}A!} \prod_{i=1}^{A} \int d^3x_i e^{-i\vec{k}_i \cdot \vec{x}_i} \psi(x_i) \delta^3\Big(\sum_{i=1}^{A} x_i\Big) \tag{2.20}$$

and

$$\frac{\Gamma'}{A\Delta^2 + \sum_{i=1}^{A} (\vec{k}_i + \vec{q}_i)^2} = \sqrt{(2m)^{A-1}A!} \prod_{i=1}^{A} \int d^3x_i e^{i(\vec{k}_i + \vec{q}_i) \cdot \vec{x}_i} \psi^*(x_i) \delta^3\Big(\sum_{i=1}^{A} (x_i)\Big).$$

We now obtain from (2.17) and (2.20) our basic formula [7, 8]

$$\mathscr{A}^{(n)} = \frac{A!}{(A-n)!n!} \prod_{i=1}^{n-1} \int \frac{d^3q_i}{(2\pi)^3 2m} V^{(n)}(s^*, \vec{q}_i) \prod_{i=1}^{A-1} \int d^3x_i e^{i\vec{q}_i \cdot \vec{x}_i} |\psi(x_i)|^2. \tag{2.21}$$

If $V^{(n)}$ does not depend on $\vec{q}_{i\mathrm{T}}$ significantly[5], the $q_{i\mathrm{T}}$ integrals can be done trivially using

$$\sum_{i=1}^{n} \vec{q}_{i\mathrm{T}} \cdot \vec{x}_{i\mathrm{T}} = \sum_{i=1}^{n-1} \vec{q}_{i\mathrm{T}}(\vec{x}_i - \vec{x}_n)_{\mathrm{T}} + \vec{q}_{\mathrm{T}} \cdot \vec{x}_{n\mathrm{T}}$$

to obtain

$$(2\pi)^{2n} \delta^2(x_{1\mathrm{T}} - x_{n\mathrm{T}}) \delta^2(x_{2\mathrm{T}} - x_{n\mathrm{T}}) \ldots \delta^2(x_{n-1\mathrm{T}} - x_{n\mathrm{T}}).$$

Writing $\vec{x}_{n\mathrm{T}} = \vec{b}$, we have [7, 8]

$$\mathscr{A}^{(n)} = \frac{A!}{(A-n)!n!} \prod_{i=1}^{n-1} \int \frac{dq_{iz}}{(2\pi)(2m)} V^{(n)}(s^*, q_{iz}) \prod_{i=1}^{n} \int dz_i e^{iq_{iz}z_i}$$

$$\times \int d^2b e^{i\vec{q}_{\mathrm{T}} \cdot \vec{b}} \varrho(\vec{b}, z_1; \vec{b}, z_2; \ldots; \vec{b}, z_n), \tag{2.22}$$

where we define

$$\prod_{j=n+1}^{A-1} \int d^3x_j |\psi(x_1, \ldots, x_A)|^2 = \varrho(x_1, \ldots, x_n). \tag{2.23}$$

---

[4] The delta function fixes the centre of mass at the origin, which is necessary since translation invariance has already been taken into account in (2.17).

[5] The condition is that the Fourier transform $\tilde{V}^{(n)}(s^*, \vec{b}_i)$ be concentrated at $\vec{b}_i$ values small compared to the nuclear size (regime (*i*)).

Equation (2.22) can be rewritten by dividing it into pieces, each of which has a definite ordering of the z_i. Assuming symmetry of $V^{(n)}$ under interchange of the q_{iz} we obtain

$$\mathscr{A}^{(n)} = \frac{A!}{(A-n)!}\prod_{i=1}^{n-1}\int\frac{dl_i}{(2\pi)(2m)}\,V^{(n)}(s^*, l_i)\int_{-\infty}^{\infty}dz_1\int_{z_1}^{\infty}dz_2 e^{il_1(z_1-z_2)}$$

$$\times\ \ldots\int_{z_{n-1}}^{\infty}dz_n e^{il_{n-1}(z_{n-1}-z_n)}\int d^2b e^{i\vec{q}_T\cdot\vec{b}}\varrho(\vec{b};\, z_i), \tag{2.24}$$

where $l_1 = q_{iz}$ and $l_k = l_{k-1}+q_{kz}$. The exponential factors allow the l_i contours to be closed in the lower half planes yielding [8]

$$\mathscr{A}^{(n)} = \frac{A!}{(A-n)!}(-2s^*)^{-n+1}\prod_{i=1}^{n-1}\int_{(M_i)^2_{\text{th}}}^{\infty}\frac{dM_i^2}{2\pi}\,\text{disc}_{M_1^2}\ldots\text{disc}_{M_{n-1}^2}V^{(n)}$$

$$\times\int_{-\infty}^{\infty}dz_1\int_{z_1}^{\infty}dz_2\exp\left[i\left(\frac{M_1^2-m_h^2}{2p}\right)(z_1-z_2)\right]\ldots$$

$$\times\int_{z_{n-1}}^{\infty}dz_n\exp\left[i\left(\frac{M_{n-1}^2-m_h^2}{2p}\right)(z_{n-1}-z_n)\right]\int d^2b e^{i\vec{q}_T\cdot\vec{b}}\varrho(\vec{b};\, z_i), \tag{2.25}$$

where $M_i^2 \equiv (p_h-l_i)^2$. This has the physical interpretation of a multiple scattering process with inelastic intermediate states as shown in Fig. 10. All the scatterings take place at the

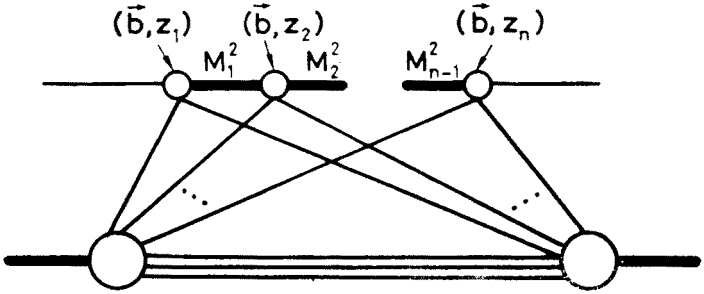

Fig. 10. Multiple scattering process corresponding to Eq. (2.25)

same impact parameter as we argued should be the case in Fig. 3. We note that if correlations between the nucleons are neglected we can write

$$\varrho(x_1, \ldots, x_n) = \prod_{i=1}^{n}\varrho(x_i), \tag{2.26}$$

where $\varrho(x)$ is the single nucleon density.

As a simple application of this formalism we consider elastic rescattering as shown in Fig. 6. For $n = 2$ and $\vec{q}_T = 0$ we have, starting from (2.21)

$$\mathscr{A}^{(2)} = \frac{A(A-1)}{2}\int \frac{d^3q_1}{(2\pi)^3 2m}\, V^{(2)}(s^*, q_{1z}) \int d^3x_1 \int d^3x_2 e^{i\vec{q}_1\cdot(\vec{x}_1-\vec{x}_2)}\varrho(x_1)\varrho(x_2), \quad (2.27)$$

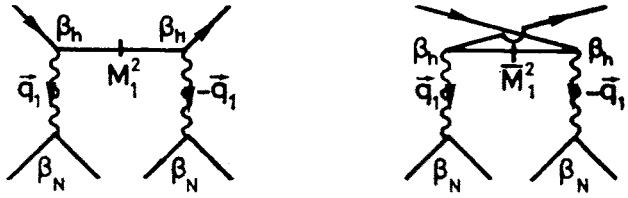

Fig. 11. Elastic contributions to $V^{(2)}$

where (see Fig. 11)

$$iV^{(2)} = \frac{i}{M_1^2 - m_h^2 + i\varepsilon}\left[(i\beta_h(-\vec{q}_1^{\,2}))\,(-i\tilde{\xi}(s^*)^{\alpha(-\vec{q}_1^{\,2})})\,(i\beta_N(-\vec{q}_1^{\,2}))\right]^2$$

$$+ \frac{i}{\bar{M}_1^2 - m_h^2 + i\varepsilon}\left[(i\beta_h(-\vec{q}_1^{\,2}))\,(-i\tilde{\xi}(s^*)^{\alpha(-\vec{q}_1^{\,2})})\,(i\beta_N(-\vec{q}_1^{\,2}))\right]^2, \quad (2.28)$$

where

$$M_1^2 = m_h^2 - \vec{q}_1^{\,2} + 2pq_{1z}, \qquad \bar{M}^2 = m_h^2 - \vec{q}_1^{\,2} - 2pq_{1z}. \quad (2.29)$$

If the singularities of the nuclear form factor in q_{1z} are neglected, the q_{1z} integral can be done simply by contour methods. Since $V^{(2)}$ behaves like q_{1z}^{-2}, a large semicircle gives no contribution and we can close around the right-hand pole obtaining[6]

$$\mathscr{A}^{(2)} = \frac{A(A-1)}{2}\,\frac{i}{2s^*}\int \frac{d^2q_{1T}}{(2\pi)^2}\left[\beta_h\tilde{\xi}(s^*)^{\alpha(-\vec{q}_{1T}^{\,2})}\beta_N\tilde{\varrho}(q_{1T}^2)\right]^2, \quad (2.30)$$

where $\tilde{\varrho}$ is the Fourier transform of the single nucleon density. This is the usual elastic absorption formula and it has the behaviour characteristic of a Regge cut[7]:

a) Asymptotic behaviour $((s^*)^{2\alpha(0)-1}/\ln s^*)$

b) Sign opposite to pole term $\mathscr{A}^{(1)}$ ($-$i for $\tilde{\xi} = $ i). (2.31)

---

[6] The same result can also be obtained starting from (2.25) which does not ignore the form factor singularities. Only in the elastic case can we get away with the neglect of these singularities — see Section 3.

[7] To avoid possible confusion, we note that since Eq. (2.28) has only pole singularities, this is not the usual AFS cut which vanishes. See Section 3 for further discussion.

It is straightforward to compute the n-fold scattering diagram in an analogous manner. In the limit of large A the optical model result is obtained from (2.1) [8]:

$$\mathscr{A}_{hA} \sim 2is^* \int d^2b e^{i\vec{q}_T \cdot \vec{b}} \left[1 - \exp\left(\frac{i}{2} \beta_h \tilde{\xi}(s^*)^{\alpha(0)-1} \beta_N A \int_{-\infty}^{\infty} dz \varrho(\vec{b}, z) \right) \right]. \tag{2.32}$$

Hence σ_{hA} is proportional to R^2 for large A as alleged in Section 1.

3. Inelastic rescattering in the Regge model

Let us analyse in detail the double-scattering diagram (Fig. 7 with $n = 2$). From Eq. (2.21) with $\vec{q} = 0$ we have

$$\mathscr{A}^{(2)} = \frac{A(A-1)}{2} \int \frac{d^3q}{(2\pi)^3 2m} V^{(2)}(s^*, q_z, \vec{q}^2)$$

$$\times \int d^3x_1 e^{i\vec{q} \cdot \vec{x}_1} \int d^3x_2 e^{-i\vec{q} \cdot \vec{x}_2} \prod_{j=3}^{A-1} \int d^3x_j |\psi(x_1, \ldots, x_A)|^2. \tag{3.1}$$

We neglect correlations between the nucleons and use (2.23) to obtain

$$\mathscr{A}^{(2)} = \frac{A(A-1)}{2} \int \frac{d^3q}{(2\pi)^3 2m} V^{(2)}(s^*, q_z, \vec{q}^2) \tilde{\varrho}(\vec{q}^2) \tilde{\varrho}(\vec{q}^2). \tag{3.2}$$

Due to the presence of ϱ the integral will be strongly damped for $|\vec{q}| \gg 1/R$[8]. Since (see Eq. (2.9))

$$M^2 \equiv (p_h - q)^2 \approx m_h^2 - \vec{q}^2 + 2pq_z, \tag{3.3}$$

we have

$$\frac{M^2}{S^*} \lesssim \frac{2p \dfrac{1}{R}}{2pm} \approx \frac{1}{mR} \approx \frac{1}{5A^{1/3}} \ll 1. \tag{3.4}$$

---

[8] The momentum cut-off here is controlled by $1/R$ and not k_F (the Fermi momentum). While it is true there are nucleons in the nucleus in states i with momenta of order k_F, $\varrho(x) \equiv (1/A) \sum_{i=1}^{A} = |\psi_i|^2$ has Fourier components only of order $1/R$. The two-particle density $\chi(x_1, x_2)$ has Fourier components of order k_F. These correspond to anticorrelations (Fermi principle) and are of weight $1/A$ with respect to the uncorrelated term since they involve only nucleons in the same state. Their total contribution to (3.3) at fixed $M^2(q_z)$ is thus of order $(1/A)(k_F^2)$ compared to $(1/R)^2$ for the uncorrelated term. Using $k_F^3 \approx A/R^3$ we see that crudely they are smaller by a factor $1/k_F R \approx 1/A^{1/3}$.

The nuclear size thus has the very important effect of restricting us to a regime where Regge exchanges are expected to dominate in $V^{(2)}$ [4, 5]. We therefore write (see Fig. 12)

$$V^{(2)} \approx \beta_N^2(t)\,(\tilde{\xi}_i(s^*)^{\alpha_i(t)})\,(\tilde{\xi}_j(s^*)^{\alpha_j(t)})F_{ij}(M^2, t), \tag{3.5}$$

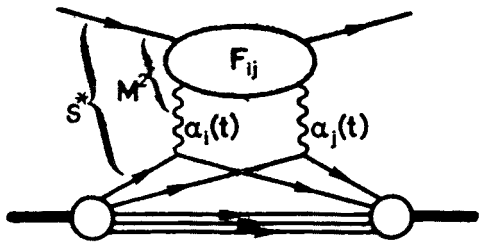

Fig. 12. Regge form for the double-scattering diagram

where F_{ij} is the Reggeon-particle scattering amplitude (the labels i and j will often be suppressed). Substituting in (3.2) gives

$$\mathscr{A}^{(2)} = \frac{A(A-1)}{4(2\pi)^3}\int_{-\infty}^{\infty} dM^2 \int d^2q_T \xi_i \xi_j (s^*)^{\alpha_i(t)+\alpha_j(t)-1} F_{ij}(M^2, t)\,(\beta_N(t)(\tilde{\varrho}-t))^2, \tag{3.6}$$

where

$$t \approx -\vec{q}^{\,2} \approx -\vec{q}_\perp^{\,2} - \left(\frac{M^2-m_h^2}{2p}\right)^2. \tag{3.7}$$

As a check of the general structure of (3.6) we note that the q_T integral will give something of order R^{-2} due to $\tilde{\varrho}$ where we assume that the nuclear dimension is much greater than typical hadronic dimensions (i. e. the t dependence of F, α, β_N can be neglected). Thus

$$\mathscr{A}^{(2)} \propto A^2 \frac{1}{R^2}\beta_N^2(0)\,(s^*)^{2\alpha(0)-1}\int_{-\infty}^{\infty} dM^2 F(M^2, 0)$$

$$\propto \frac{1}{s^*}(A\beta_N(s^*)^{\alpha(0)})\,(A^{1/3}\beta_N(s^*)^{\alpha(0)})\int_{-\infty}^{\infty} dM^2 F(M^2, 0).$$

The factor $A\beta_N(s^*)^{\alpha(0)}$ is due to the first interaction which can take place with any of the A nucleons, while the factor $A^{1/3}\,\beta_N(s^*)^{\alpha(0)}$ is due to the second interaction which can take place only with the approximately $A^{1/3}$ nucleons with the same transverse coordinate as the first struck nucleon. The integral measures the total weight of elastic and inelastic diffractive states propagating between the interactions.

Further insight into the physical meaning of the double-scattering diagram can be gained if we consider its contribution to the total hadron-nucleus cross-section. This is obtained by taking the imaginary part or, equivalently, according to Cutkosky, by summing over all unitarity cuts which divide the diagram into two pieces. We therefore can write

$$s\sigma_{hA}^{\mathrm{tot}\,(2)} = \frac{1}{2i}\left[(\mathrm{disc}\,\mathscr{A}^{(2)})_0 + (\mathrm{disc}\,\mathscr{A}^{(2)})_1 + (\mathrm{disc}\,\mathscr{A}^{(2)})_2\right], \tag{3.8}$$

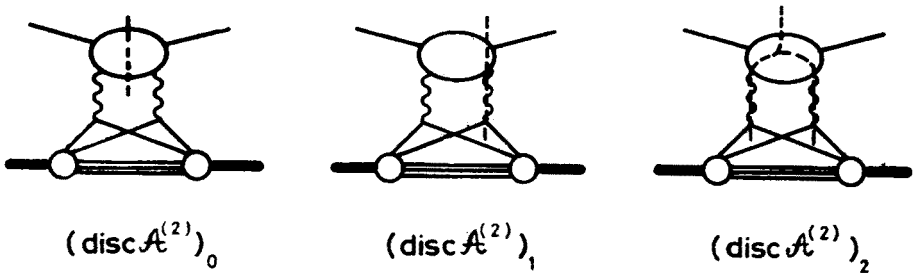

Fig. 13. Contributions to the various discontinuities of $\mathscr{A}^{(2)}$

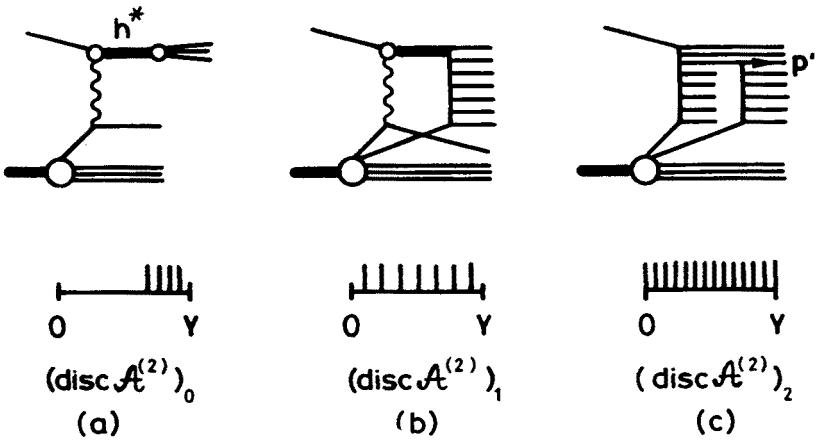

Fig. 14. Examples of production processes and rapidity distributions (the A nucleons excluded) contributing to [disc $\mathscr{A}^{(2)}$]$_i$

where the (disc $\mathscr{A}^{(2)}$)$_i$ contain all terms where i Reggeons have been cut (see Fig. 13). An example of a specific production process contributing to each of these discontinuities is shown in Fig. 14. Contributions to the cut through no Reggeons are generally diffractive dissociation processes. Contributions to the cut through one Reggeon include absorbed multiperipheral processes as well as the basic process of Fig. 5a. Contributions to the cut through both Reggeons are what would normally be called double-scattering processes. After a scattering off one nucleon, one of the produced particles scatters off a second nucleon. The double-scattering diagram therefore includes the contributions of many distinct production processes. The outstanding feature of Regge theory is that all these

processes are related to each other in such a way that unitarity is satisfied (this is most clear if we imagine all diagrams to consist of sums of Feynman diagrams [10]).

We now turn to a detailed analysis of the double-scattering diagram. The M^2 contour in (3.6) cannot simply be closed around the righ-hand (or left-hand) singularities in $F(M^2, t)$ which arise from unitarity in the Reggeon-particle channel. This is because there are

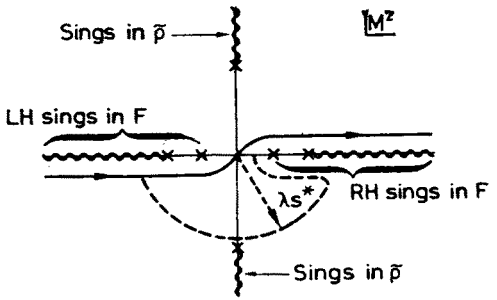

Fig. 15. Singularities in the M^2 complex plane. The dotted line is the integration contour used in obtaining Eq. (3.11)

additional singularities in M^2 arising from the q_z dependence of $\tilde{\varrho}$ (see Fig. 15). Therefore $\mathscr{A}^{(2)}$ cannot be expressed simply in terms of $\mathrm{disc}_{M^2}F$ (or $\mathrm{disc}_{M^2}V^{(2)}$) and it is most convenient to evaluate the contour integral directly[9].

Let us choose a number λ such that

$$\lambda \ll \frac{1}{mR} \quad \text{but} \quad \lambda s^* \gg m^2. \tag{3.9}$$

This will generally be possible for high energies. Then for $|M^2|/s^* \leqslant \lambda$ we are in a regime where

$$|M^2 - m_h^2|/2p \ll \frac{1}{R}$$

and $t \approx -\vec{q}_T^2$. The only M^2 dependence in (3.6) then occurs in $F(M^2, t)$. Let us consider

$$\int_{-\lambda s^*}^{\lambda s^*} dM^2 F(M^2, t). \tag{3.10}$$

Using Cauchy's theorem the integral can be rewritten as (see Fig. 15)

$$\int_{M_0^2}^{\lambda s^*} dM^2\, \mathrm{disc}_{M^2}F(M^2, t) + \int_{|M^2|=\lambda s^*} dM^2 F(M^2, t). \tag{3.11}$$

---

[9] An alternative approach is to start from Eq. (2.25). Then only the $\mathrm{disc}_{M^2}V^{(3)}$ is involved but a complicated nuclear "form factor" occurs.

Since $\lambda s^* \gg m^2$ we can use the triple-Regge form for F in the second term in (3.11) (see Fig. 16)[10]:

$$F_{ij}(M^2, t) \sim \beta_h(0) \frac{[e^{-i\pi(\alpha_k(0)-\alpha_i(t)\alpha_j(-t)} + \tau_i\tau_j\tau_k]}{-\sin \pi(\alpha_k(0)-\alpha_i(t)-\alpha_j(t))} (M^2)^{\alpha_k(0)-\alpha_i(t)-\alpha_j(t)} g_{ijk}(t). \tag{3.12}$$

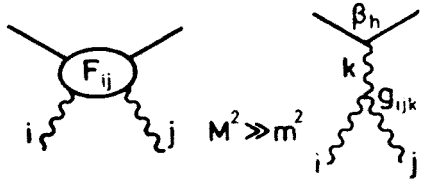

Fig. 16. Triple-Regge limit of F_{ij}

Hence the second term has the behaviour $(s^*)^{\alpha_k(0)-\alpha_i(t)-\alpha_j(t)+1}$ which, when inserted in (3.7), gives a behaviour $(s^*)^{\alpha_k(0)}$. It is therefore a contribution to the renormalization of the α_k Regge-pole reside due to nuclear rescattering. Breaking the first integral into two parts at some Λ ($m^2 \ll \Lambda \leqslant \lambda s^*$) we obtain

$$\int_{M_0^2}^{\Lambda} dM^2 \operatorname{disc}_{M^2} F_{ij}(M^2, t) + \int_{\Lambda}^{\lambda s^*} dM^2 [2i\beta_h(0) g_{ijk}(t) (M^2)^{\alpha_k(0)-\alpha_i(t)-\alpha_j(t)}]$$

$$= 2i \left[\int_{M_0^2}^{\Lambda} dM^2 \operatorname{Im} F_{ij}(M^2, t) - \frac{\Lambda^{\alpha_k(0)+1-\alpha_i(t)-\alpha_j(t)}}{\alpha_k(0)+1-\alpha_i(t)-\alpha_j(t)} \beta_h(0) g_{ijk}(t) \right]$$

$$+ 2i \frac{(\lambda s^*)^{\alpha_k(0)+1-\alpha_i(t)-\alpha_j(t)}}{\alpha_k(0)+1-\alpha_i(t)-\alpha_j(t)} \beta_h(0) g_{ijk}(t). \tag{3.13}$$

The last term is again a residue renormalization. Hence we can write (3.7) as

$$\mathscr{A}^{(2)} = \frac{A(A-1)}{16\pi^2} i \int dt \tilde{\xi}_i \tilde{\xi}_j (s^*)^{2\alpha(t)-1} (\beta_N(t)\tilde{\varrho}(-t))^2$$

$$\times \frac{1}{\pi} \left[\int_{M_0^2}^{\Lambda} dM^2 \operatorname{Im} F_{ij}(M^2, t) - \frac{\Lambda^{\alpha_k(0)+1-\alpha_i(t)-\alpha_j(t)}}{\alpha_k(0)+1-\alpha_i(t)-\alpha_j(t)} \beta_h(0) g_{ijk}(t) \right] + f(A) (s^*)^{\alpha_k(0)}. \tag{3.14}$$

where $t \approx -\vec{q}_T^{\,2}$.

---

[10] Strictly speaking only part of the triple-Regge limit of $V^{(2)}$ is given here (see Ref. [11]). This point is discussed further below (see Eq. (3.22)).

Let us discuss the two terms in Eq. (3.14) successively. The first term has the behaviour (2.31) and is the standard Regge-cut contribution (for an excellent review see Ref. [6]). The quantity in brackets

$$N_{ij}(t) \equiv \frac{1}{\pi}\left[\int_{M_0^2}^{\Lambda} dM^2 \,\mathrm{Im}\, F_{ij}(M^2, t) - \frac{\Lambda^{\alpha_k(0)+1-\alpha_i(t)-\alpha_j(t)}}{\alpha_k(0)+1-\alpha_i(t)-\alpha_j(t)} \beta_h(0) g_{ijk}(t)\right] \tag{3.15}$$

is the subtracted sum rule [12] for the fixed pole residue defined by Gribov [10].

It is interesting to ask under what conditions this term can have the elastic (Glauber) form of Eq. (2.30) since empirically it appears the Glauber formula gives a rough fit to the total cross-section data. The elastic contribution will dominate if Im $F(M^2, t) \approx \pi\delta(M^2 - m_h^2)\,\beta_h^2(t)$ (i. e. diffractive inelastic excitation is small) and the subtraction term is negligible. The latter is true if $\alpha_k(0)+1-\alpha_i(t)-\alpha_j(t) < 0$ and/or g_{ijk} is small.

These conditions cannot be met if $F(M^2, t)$ is constructed only from planar Feynman diagrams, since in this case the cut vanishes identically due to the AFS cancellation mechanism [13] (see Appendix). The simplest planar graph is shown in Fig. 17a. It gives contribu-

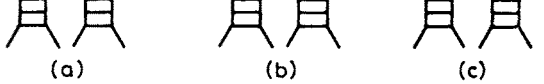

Fig. 17. Planar Feynman diagrams contributing to $V^{(2)}$

tions to Im F coming from cuts of the type shown in Fig. 17b. In addition to the elastic pole there are inelastic contributions coming from cuts through a finite number of rungs of either ladder. The latter are negative and exactly cancel the elastic contribution in (3.15) (see solid line in Fig. 18) [14]. For this diagram the discontinuity of the forward Reggeon-

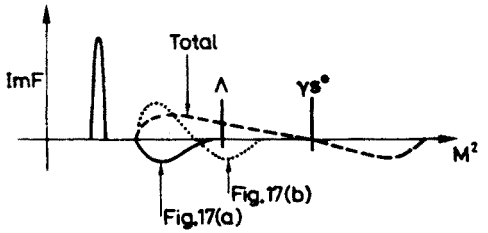

Fig. 18. Contributions to Im $F(M^2, t)$ from planar graphs

-particle amplitude $F(M^2, t)$ is not positive definite so it cannot be the whole story. To restore positivity other diagrams such as Fig. 17c must be included. If we assume that the series of all ladder diagrams in the hh channel, of which Figs 17a and 17c are the first members, produces a Regge pole α_k and satisfies positivity in the triple-Regge region, we obtain a picture as shown in the dashed line of Fig. 18 [15]. If $\alpha_i(0) = \alpha_j(0) = \alpha_k(0) \leqslant 1$,

the fixed pole residue must vanish identically due to an exact cancellation between the integral and the subtraction term. The subtraction term thus has a weight equal to or greater than the Glauber term and is therefore not negligible. Therefore the approximate validity of the Glauber series at current energies does not imply the dominance of planar Feynman graphs[11]. On the contrary, it means there must be significant contributions from non-planar graphs. Diagrams such as Fig. 10 with only elastic states represent dispersion integrals (see Eq. (2.25)) and should not be confused with planar Feynman graphs[12].

The second term in Eq. (3.14), which contains the remaining part of the M^2 integral in (3.6) as well as the second terms in (3.11) and (3.13), gives a contribution to the nuclear

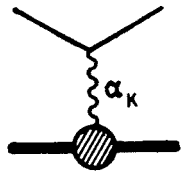

Fig. 19. Nuclear Regge residue

Regge residue (Fig. 19). It is difficult to evaluate, since the longitudinal component of the momentum transfer q_z cannot be neglected. Let us attempt to discuss it qualitatively, however.

As a simple model we take the triple-Regge form (3.12) for F and compute only the contribution to (3.6) arising from the singularities in F,

$$\mathscr{A}^{(2)} \approx i\frac{A(A-1)}{16\pi^2}\int_{M_0^2}^{\infty} dM^2 \int dq_T^2 \xi_i \xi_j (s^*)^{\alpha_i(t)+\alpha_j(t)-1} \operatorname{Im} F_{ij}(M^2, t)\,(\beta_N(t)\tilde{\varrho}(-t))^2$$

$$\approx c\frac{A^2}{R^2}\int_{M_0^2}^{\infty} dM^2 (s^*)^{2\alpha(0)-1}(M^2)^{\alpha_k(0)+1-\alpha_i(0)-\alpha_j(0)} e^{-\frac{R^2M^2}{2p}}$$

$$\approx \left[c'\frac{A^2}{R^2}\int_0^Y dy e^{-y(\alpha_k(0)+1-\alpha_i(0)-\alpha_j(0))} e^{-(Rme^{-y})^2}\right](s^*)^{\alpha_k(0)}, \tag{3.16}$$

where we have introduced

$$M^2 = \frac{m^2}{2}e^{Y-y}, \qquad p = \frac{m}{2}e^{Y} \tag{3.17}$$

---

[11] The suggestion in Ref. [16] that the planar dual model might provide a good approximation is untenable for these reasons.

[12] The decomposition of F into contributions from planar and non-planar Feynman graphs was made only for illustrative purposes. I do not believe it has much utility since we do not have a specific underlying field theory for stros interactionng.

and assumed the simple form $[\tilde{\varrho}(q^2)]^2 = \exp(-q^2R^2)$. The variable y can be interpreted as the rapidity of the produced particle which undergoes the second scattering which generates the triple-Regge contribution ($p' = (m/2)\, e^y$ in Fig. 14). We can interpret the integrand of Eq. (3.17) as giving the probability that the rescattering occurs for a particle of momentum p'. It is plotted in Fig. 20 for the case $\alpha_i(0) = \alpha_j(0) = \alpha_k(0) \equiv \alpha(0) < 1$. We see that it

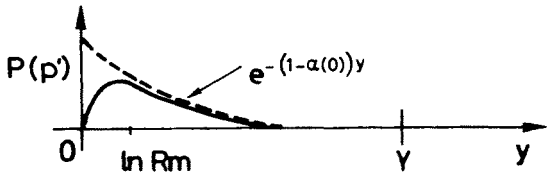

Fig. 20. Rescattering probability as a function of rapidity y of rescattered particle

peaks for $y \approx \ln Rm$. In this case rescatterings are restricted to particles of momenta $p' \leqslant m^2R$. For momenta above $p' \approx m^2R$ there is only the simple multiperipheral process giving Regge behaviour in the energy p/R across the chain. For momenta below $p' \approx m^2R$ there are complicated rescattering processes, the simplest example of which we have just discussed. *If* these rescattering processes lead to a strong enough absorption we can expect a geometrical amplitude proportional to R^2 for these processes[13]. Therefore we have for the pole contribution [16],

$$s\sigma_{hA}^{tot} \approx \left(\frac{p}{m^2R}\right)^{\alpha(0)} R^2 \tag{3.18}$$

for $\alpha(0) < 1$. This is smaller than (1.11) which would give

$$s\sigma_{hA}^{tot} \propto \frac{\frac{1}{\sigma_{hN}} R^2}{R^3} As\sigma_{hN} \propto \left(\frac{p}{m}\right) R^2.$$

The reason is that the dominant rescattering is that of relatively slow produced particles ($p' \leqslant p$) rather than that of the fast leading particle as in the simple elastic rescattering model. The absorption is greater since the low-energy cross-section is larger [$\alpha(0) < 1$!]. Empirically, the difference between the two formulae will be insignificant since $\alpha(0) \approx 1$.

We conclude this section by considering a more sophisticated example of Regge residue renormalization. It will clarify a number of technical points including obtaining the correct phase $\tilde{\xi}_k$ for the power $(s^*)^{\alpha_k}$ which was not obtained in Eq. (3.16).

We consider the following simple forms

$$\tilde{\varrho}^2(\vec{q}^{\,2}) = \frac{1}{1 + R^2\vec{q}^{\,2}} \tag{3.19}$$

[13] This may not be the case for reasonable A, see discussion below Eq. (5.12).

and

$$F_{ij}(M^2, t) = \tilde{F}_{ij}(M^2, t) + \tau_i\tau_j\tau_k\tilde{F}_{ij}(-M^2, t), \tag{3.20}$$

where[14]

$$\tilde{F}_{ij}(M^2, t) = \frac{1}{\pi}\int_A^{\varepsilon s^*} \frac{dM'^2}{M'^2 - M^2}\,(M'^2)^{\alpha_k(0)-\alpha_i(t)-\alpha_j(t)}\beta_h(0)g_{ijk}(t). \tag{3.21}$$

The expression for the "signatured" amplitude $\tilde{F}$ is a dispersion relation which includes the region where the triple-Regge form (3.12) holds. For $A < M^2 < \varepsilon s^*$ we have

$$\begin{aligned}\tilde{F}(s^*)^{\alpha_i+\alpha_j} &= \frac{\beta g(-M^2)^{\alpha_k-\alpha_i-\alpha_j}}{-\sin\pi(\alpha_k-\alpha_i-\alpha_j)}(s^*)^{\alpha_i+\alpha_j} \\ &+ \frac{1}{\pi}\sum_{I=0}^{\infty}\frac{\varepsilon^{\alpha_k-\alpha_i-\alpha_j-I}}{\alpha_k-\alpha_i-\alpha_j-I}\beta g\left(\frac{M^2}{s^*}\right)^I(s^*)^{\alpha_k} \\ &- \frac{1}{\pi}\sum_{I=-1}^{-\infty}\frac{A^{\alpha_k-\alpha_i-\alpha_j-I}}{\alpha_k-\alpha_i-\alpha_j-I}\beta g(-M^2)^I(s^*)^{\alpha_i+\alpha_j}.\end{aligned} \tag{3.22}$$

The full amplitude can have no singularities for integral $\alpha_k-\alpha_i-\alpha_j$ since these do not correspond to physical particles. The second sum contains "fixed poles" (which contribute to Eq. (3.15) for $I = -1$) cancelling these singularities for negative integers. The first sum contains terms which contribute to Regge residue renormalization and cancel these singularities for non-negative integers.

The integral (3.2) can be done explicitly by closing the contour in the lower half plane ($\alpha_k-\alpha_i-\alpha_j < 1$):

$$\begin{aligned}\mathscr{A}^{(2)} = \frac{A(A-1)}{2}\int\frac{d^2q_T}{(2\pi)^2}\Bigg[\frac{i}{\pi}\int_A^{\varepsilon s^*}\frac{dM'^2}{2s^*}(M'^2)^{\alpha_k-\alpha_i-\alpha_j}\frac{1}{R^2/R_T^2+R^2\left(\dfrac{M'^2}{2p}\right)^2} \\ + \frac{1}{4m}F_{ij}\left(-2ip\frac{1}{R_T}\right)\frac{R_T}{R^2}\Bigg]\beta_h g_{ijk}\beta_N^2\tilde{\xi}_i\tilde{\xi}_j(s^*)^{\alpha_i+\alpha_j}\end{aligned} \tag{3.23}$$

where

$$\frac{1}{R_T^2} = \frac{1}{R^2} + q_T^2.$$

[14] This example is discussed in Section 6.3 of Ref. [11]. We take $\tau_i\tau_j\tau_k = +1$, since otherwise the contribution to (3.2) vanishes.

For $\alpha_k-\alpha_i-\alpha_j < -1$[15] the integral is well behaved at the lower end point and using (3.22) we have

$$\mathscr{A}^{(2)} = \frac{A(A-1)}{4m}\int\frac{d^2q_T}{(2\pi)^2}\,\frac{R_T}{R^2}\left[\frac{-i\sin\frac{\pi}{2}(\alpha_k-\alpha_i-\alpha_j)}{-\sin\pi(\alpha_k-\alpha_i-\alpha_j)}(mR_T)^{\alpha_i+\alpha_j-\alpha_k}\right.$$

$$+\frac{\cos\frac{\pi}{2}(\alpha_k-\alpha_i-\alpha_j)}{-\sin\pi(\alpha_k-\alpha_i-\alpha_j)}(mR_T)^{\alpha_i+\alpha_j-\alpha_k}$$

$$\left.+\frac{1}{\pi}\,\frac{\varepsilon^{\alpha_k-\alpha_i-\alpha_j}}{\alpha_k-\alpha_i-\alpha_j}+O\left(\frac{1}{\varepsilon R_T m}\right)\right]\beta_h g_{ijk}\beta_N^2\tilde{\xi}_i\tilde{\xi}_j(s^*)^{\alpha_k}$$

$$+\text{Regge cut subtraction term.} \tag{3.24}$$

The first two terms have the phase $e^{i(\pi/2)\alpha_k}$ appropriate to the Regge pole behaviour $(s^*)^{\alpha_k}$. The third term cancels the singularity in the first two terms at $\alpha_k-\alpha_i-\alpha_j = 0$. (Only the value of its singularity should be taken seriously, since its non-singular part depends on the artificial cut-off parameter ε and will receive contributions from $M'^2 > \varepsilon s^*$ in general.) Thus this contribution to the Regge amplitude is perfectly well behaved[16]. It also has the characteristic behaviour $(s^*/mR)^{\alpha_k}f(R)$ discussed above Eq. (3.18). One should keep in mind, however, that the triple-Regge contributions give only part of the residue renormalization. There can be significant contributions coming from $M^2 > \varepsilon s^*$ in $V^{(2)}$ where the triple-Regge form does not hold.

4. *Multiparticle production*

At the beginning of Section 3 we discussed the contribution of the double-scattering diagram (Fig. 12) to the total hadron-nucleus cross-section. One way to obtain the contribution is just to take the imaginary part of Eq. (3.6) or, alternatively, Eq. (3.14). From the latter equation we see that the Pomeron-Pomeron cut contribution gives a term

$$\mathscr{A}^{(2)} \propto i(i)\,(i) = -i$$

and thus a negative contribution to $\sigma_{hA}^{\text{tot}(2)}$. On the other hand, from general analyticity properties we have $\text{Im}\,\mathscr{A}^{(2)} = 1/2i\ \text{disc}_s\,\mathscr{A}^{(2)}$. The discontinuity can be expressed as a sum over all ways of cutting the diagram as shown in Fig. 13 and these have the interpretation as the contribution of various elastic and multiparticle production processes to $\text{disc}_s\,\mathscr{A}^{(3)}$ and thus $\sigma_{hA}^{\text{tot}(2)}$. Therefore, Eq. (3.1) provides a decomposition of the total cross-section contribution in terms of various classes of production processes each of which has a distinctive rapidity distribution (Fig. 14).

---

[15] For $\alpha_k-\alpha_i-\alpha_j = -1$ the separation into pole and cut terms is impossible unless $g_{ijk}(0) = 0$.

[16] $\mathscr{A}^2$ is never singular (even if $\alpha_k = 1$, $\alpha_i = \alpha_j = \frac{1}{2}$) contrary to the claims of some authors.

Perhaps the simplest question we can ask about multiparticle production is: What is the relative contribution of these three different classes of processes to σ_{hA}^{tot}? Amazingly enough, this has a simple answer. Abramovskii, Gribov and Kancheli [18] (AGK) argued that for the Regge cut contribution in (3.14)

$$\begin{aligned}
\text{disc } \mathscr{A}^{(2)} &\propto 2i \text{ Im } (i\tilde{\xi}_i\tilde{\xi}_j), \\
(\text{disc } \mathscr{A}^{(2)})_0 &\propto i(i\tilde{\xi}_i)\,(i\tilde{\xi}_j)^* + i(i\xi_i)^*(i\tilde{\xi}_j), \\
(\text{disc } \mathscr{A}^{(2)})_1 &\propto -8i(\text{Im } \tilde{\xi}_i)\,(\text{Im } \tilde{\xi}_j), \\
(\text{disc } \mathscr{A}^{(2)})_2 &\propto 4i(\text{Im } \tilde{\xi}_i)\,(\text{Im } \tilde{\xi}_j).
\end{aligned} \tag{4.1}$$

For the case of Pomerons these terms are in the ratio

$$-1 = +1-4+2. \tag{4.2}$$

Therefore, the double-scattering processes (Fig. 14c) contribute just twice as much to the cross-section as do the diffractive dissociation processes (Fig. 14a). Furthermore, a certain amount of absorption is required for the multiperipheral processes (Fig. 14b).

Arguments for the AGK rules (4.1) have been given within the framework of Feynman graphs as discussed here [6, 14, 17–19] for dual models [20], and using only the general structure of multi-Regge amplitudes [21]. There is therefore impressive theoretical support for them.

There is a simple mnemonic for the AGK result: the integrand of the cut contribution in Eq. (3.14) is the product of three factors; the Reggeon-particle coupling $N_{ij}(t)$, describing the upper part of the diagram; the Reggeon-nucleus coupling $[\beta_N(t)\,\tilde{\varrho}(-t)]^2$, describing the lower part of the diagram; and the Regge propagators $\xi_i\xi_j\, s^{\alpha_i+\alpha_j}$ linking the two parts. According to AGK the only effect of taking discontinuities is to replace the Regge propagators which have been cut through by $2i$ Im ξ_l and complex conjugate those occurring after the cut[17]. The Reggeon-patricle (or Reggeon-nucleus) couplings are not affected by the taking of the discontinuities. The derivation of this result depends crucially on the factorized form noted above. We recall that we obtained this form under the condition that (3.9) holds, which implies

$$m^2R \ll p. \tag{4.3}$$

When $p \leqslant m^2R$ the longitudinal component of momentum transfer q_z is no longer negligible compared to $|\vec{q}_T|$ and factorization and the AGK rules fail (see also the Appendix). This fact will be of great importance in what follows.

In Section 3 we emphasized that elastic (Glauber) rescattering being a good approximation does not imply the dominance of planar Feynman graphs. This becomes particularly clear in the present discussion. Planar graphs have no cuts through two Reggeons and the cutting rules

$$-1 = +1-2+0$$

[17] The cut through no Reggeons is not determined by this rule and is most easily obtained by taking the difference between the total discontinuity and the sum of the discontinuities through $n \geqslant 1$ Reggeons.

(neglecting the fact that each term is actually zero). Although elastic rescattering may be a good approximation for σ^{tot}, as long as (4.3) is satisfied the various contributions have the AGK ratios (4.2) which are typical of non-planar graphs!

We now turn from the totally inclusive cross-section to the single-particle inclusive cross-section which is the next simplest quantity to consider. Before discussing hadron--nucleus scattering, we rewiew the situation for hadron-hadron scattering.

4.1. Single-particle inclusive cross-sections: hadron-hadron scattering

Suppose a rather fast particle produced in the multiperipheral process of Fig. 5a is detected (Fig. 21a) (i.e. a particle in the central region),

$$m \ll p' \ll p \tag{4.4}$$

or

$$\Delta < y < Y - \Delta.$$

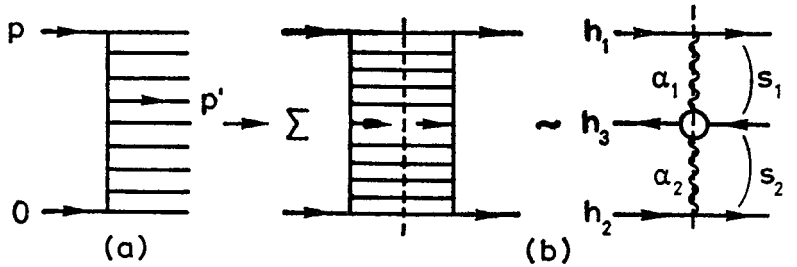

Fig. 21. Contribution to inclusive cross-section from simplest multiperipheral process

The inclusive cross-section is given by the Mueller–Regge formula of Fig. 21b (see, for example, Ref. [11])

$$s\frac{d\sigma}{d^3p'/E'} = s\frac{d\sigma}{d^2p_T dy} \sim \beta_{h_1}(0)\,\mathrm{Im}\,\tilde{\xi}_1 s_1^{\alpha_1(0)} G_{12}^{h_3}(p_T'^2)\,\mathrm{Im}\,\tilde{\xi}_2 s_2^{\alpha_2(0)}\beta_{h_2}(0). \tag{4.5}$$

Fast particles can also be produced in processes in which there is a rescattering off the "constituents" of the hadrons (for example the analogues of Figs 14b and 14c: see Fig. 22).

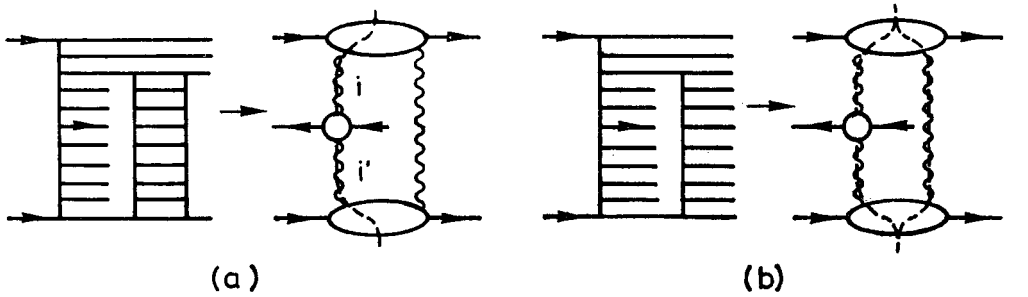

Fig. 22. Contributions to inclusive cross-section from a) absorbed multiperipheral process and b) double scattering process

We can see that just as the total cross-section can be expressed as a sum of all multi-Regge exchange contributions to the four-particle amplitude, the single-particle inclusive cross--section can be expressed as a sum of all multi-Regge exchange contributions to the six--particle amplitude. In Fig. 22 we see one possible double-Regge contribution; we discuss others below.

The evaluation of the discontinuities in Fig. 22 proceeds exactly like that of those in Fig. 13 which gives (4.1). We have only the replacement

$$\operatorname{Im} \tilde{\xi}_i \to \operatorname{Im} \tilde{\xi}_i G_{ii'}^{h_3}(p_\perp'^2) \operatorname{Im} \tilde{\xi}_{i'}$$

which is the same as that which occurs in passing from the total cross-section to (4.5). There is one crucial difference with (4.1) however: the weight of the cut through one Reggeon term is only half as large since now the cut must always be through the Reggeon from which the particle h_3 is produced, whereas in Fig. 13 it can be through either Reggeon. From (4.1) we see that the sum of Figs 22a and 22b vanishes [17]. Therefore, this double--Regge diagram gives no contribution to the single-particle inclusive cross-section in the central region. Likewise, the analogous multi-Regge diagrams give no contributions.

There are, however, some multi-Regge diagrams which do not give vanishing contributions in the central region (see Fig. 23). These are generally neglected since they correspond

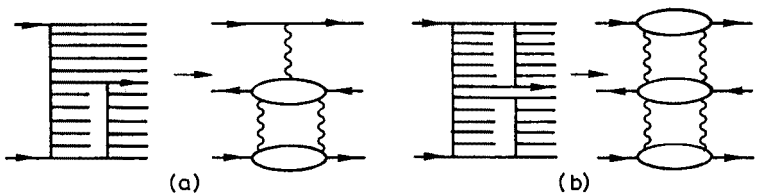

Fig. 23. Non-vanishing cut contributions in the central region

to particle production in high mass single diffractive dissociation or through double Pomeron exchange which empirically are small. Also, they lead to long-range correlations in the central region which experimentally are small compared to the short-range correlations. I shall be content to accept this conventional lore in the following.

In the fragmentation regions

$$\begin{aligned} 0 &\lesssim y \lesssim \Delta, \\ Y-\Delta &\lesssim y \leqslant Y, \end{aligned} \tag{4.6}$$

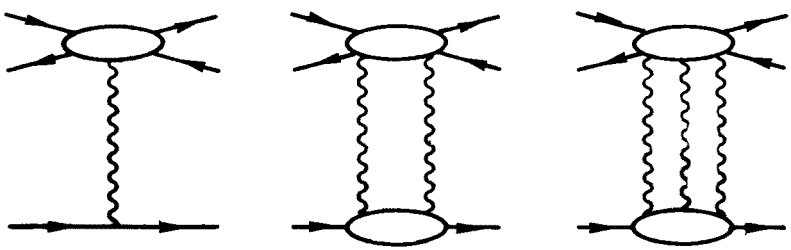

Fig. 24. Contribution to inclusive cross-section in the fragmentation region

the AGK cancellation mechanism does not operate and the discontinuities of diagrams like those in Fig. 24 contribute. These can be expected to contribute roughly in the same proportions as the corresponding Regge-cut diagrams for the elastic amplitude.

4.2. Single-particle inclusive cross-sections: hadron-nucleus scattering

All the above discussion carries over directly to the hadron-nucleus case including the vanishing of multi-Regge exchange diagrams of the form Fig. 22 in the central region with the exception of one interesting modification [22, 23]. The central region no longer extends down to $y \approx \Delta$ but only to $y \approx \ln Rm + \Delta'$. To see this, recall that we emphasized that the AGK rules fail for the elastic amplitude when (4.3) is violated due to the importance

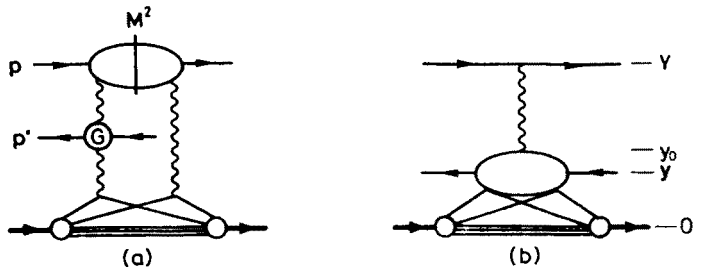

Fig. 25. Contributions to inclusive cross-section and the target fragmentation region

of the longitudinal momentum transfer which destroys the factorization into upper and lower blobs of Eq. (3.14). A similar phenomenon occurs for the diagram of Fig. 25a when $M^2 \geqslant p/R$, since again the longitudinal momentum transfer becomes important. Therefore diagrams like those of Fig. 25b will lead to A-dependent rescattering corrections when

$$y \leqslant y_0 \equiv \ln Rm + \Delta'. \tag{4.7}$$

(This is consistent with the picture of Fig. 20 for the special case $\alpha(0) < 1$ where we saw the dominant rescattering was for such values of rapidity (see also the Appendix).)

We now summarize the results of this section. Diagrams contributing to the elastic amplitude are shown in Fig. 26. In the blobs representing the Reggeon-hadron interactions the energies $|M_i^2| \leqslant A$ where A is the energy at which Regge behaviour sets in. The contributions for $|M_i^2| < A$ are taken into account by triple-Regge diagrams (compare (b) and (d), (b) and (f), and (d) and (g)). When there is scattering off more than one nucleon ((c), (e), (h), etc.) for simplicity we have always represented it as occurring through Regge exchanges since owing to (3.4) these are enhanced compared to an arbitrary general interaction of the form of Fig. 25b. When the rapidity y of the triple-Regge vertices, like those in (e) and (i), is less than y_0, the vertex is inside the nuclear fragmentation region and simple expressions like those in Section 3 no longer hold.

For phenomenological purposes it is most convenient to expand in the number of rescatterings n rather than the number of Regge exchanges as we did in Fig. 26. Thus the

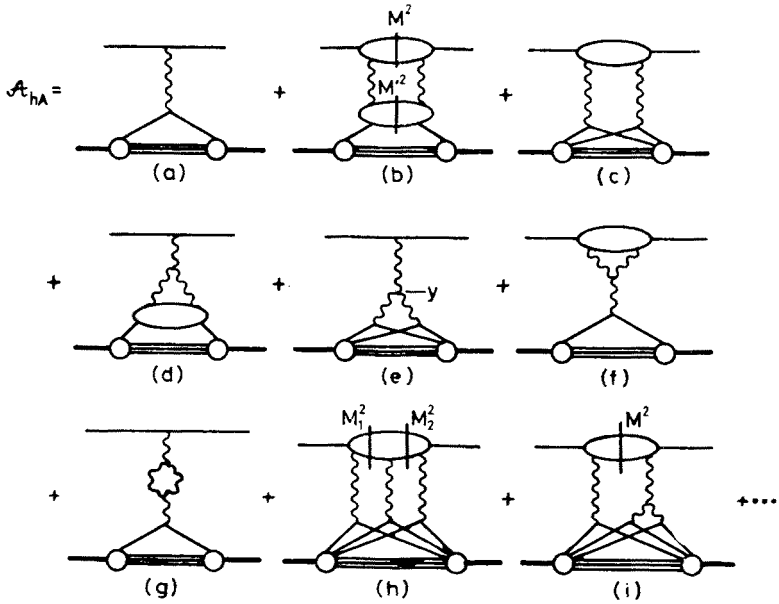

Fig. 26. Multi-Regge exchange contributions to $\mathcal{A}_{hA}$

contributions of Fig. 26a, b, d, f, and g are grouped together. We can then express $\mathcal{A}_{hA}$ as shown in Fig. 27, where the exchanges represent the full hadron-nucleon amplitude. It is amusing that a generalization of the AGK rules holds for this expansion. For example, the ratio of the three types of cuts (Fig. 13) of Figs 27b and c is still given by (4.1) with Im $\tilde{\xi}_i$ replaced by the imaginary part of the *full* hadron-nucleon amplitude [24].

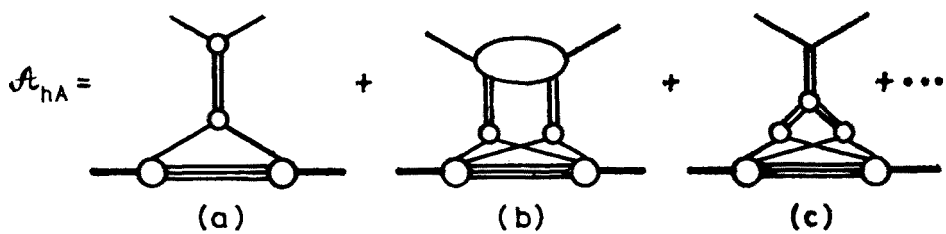

Fig. 27. Expression for $\mathcal{A}_{hA}$ in terms of number of rescatterings. The double line represents the sum of all multi-Regge exchanges to the hadron-nucleon amplitude

Diagrams contributing to the single-particle inclusive cross-section are shown in Fig. 28. Reggeon interaction terms (Fig. 23) have been omitted.

In order to gain some insight into the implications of these complicated expressions we consider two simple examples. As we shall see in Section 5, neither one is expected to be applicable at present energies, so they are considered only for illustrative purposes.

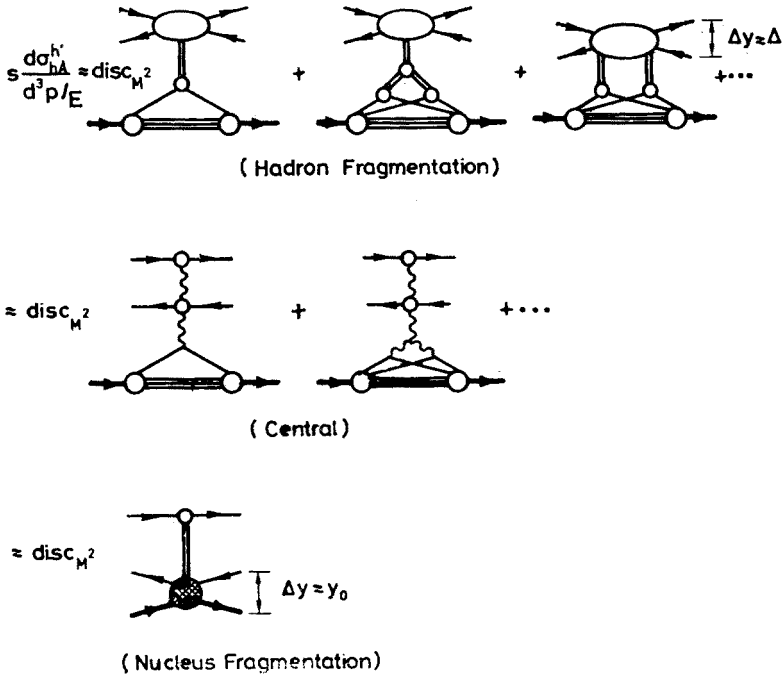

Fig. 28. Diagrams contributing to single-particle inclusive cross-section

First, suppose $\alpha_P(0) < 1$[18]. At very high energies $[1-\alpha(0)] \ln s \gg 1$, the Regge-cut contributions are negligible compared to the Regge pole and only the first two terms in Figs 27 and 28 remain. We then obtain the behaviour of the single-particle spectra shown in Fig. 29. In the hadron fragmentation region and the central region the spectrum is

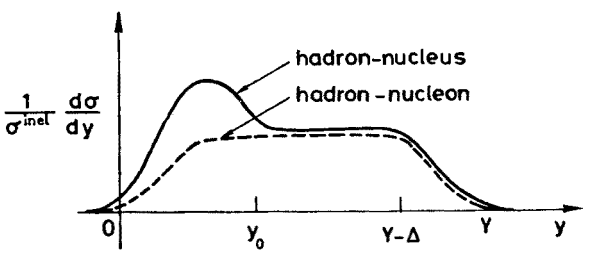

Fig. 29. Single-particle spectra for $\alpha_P(0) < 1$ and extreme energies

independent of A since both $d\sigma/dy$ and $\sigma^{inel} \sim \sigma^{tot}$ are proportional to the nuclear Regge residue. A dependence occurs for $y < y_0$, where rescatterings become important. Here we may expect a value proportional to $A^{1/3}$ or larger, since each particle with $y < y_0$

[18] Similar conclusions hold if $\alpha(0) = 1$ and $g_{PPP}(0) = 0$. This is essentially the case considered in Ref. [23].

can rescatter a number of times proportional to $A^{1/3}$. Integrating over y we obtain the total multiplicity

$$n^{h'}(A, Y) = a_h^{h'} + c^{h'}(Y - y_0) + a^{h'}(A). \tag{4.8}$$

As a second illustrative example we consider $\alpha_P(0) \approx 1$, $g_{PPP}(0) \neq 0$ and A very large. Let us first compute the contribution of the graph in Fig. 26e. From (2.27), (3.5) and (3.12) we have[19]

$$\mathscr{A}^{(2)} = -\frac{A(A-1)}{16\pi^2} \int_{-\infty}^{0} d^2 q_T \int_{A/s}^{\varepsilon} d \frac{M^2}{s} \left(\frac{M^2}{s}\right)^{\alpha_P(0) - 2\alpha_P(t)} s^{\alpha_P(0)}$$

$$\times \beta_h(0) g_{PPP}(t) \beta_N^2(t) \tilde{\varrho}^2 \left(q_T^2 + \left(\frac{M^2}{2p}\right)^2\right). \tag{4.9}$$

The nuclear factor restricts the integral to $M^2/2p \lesssim 1/R$ and we have

$$\sigma^{(2)} \approx -\frac{A^2}{R^2} \frac{\beta_h(0)\beta_N^2(0) g_{PPP}(0)}{16\pi^2} \ln \frac{s^*}{AmR}. \tag{4.10}$$

Comparing with the single-Regge exchange term of Fig. 26a

$$\sigma^{(1)} \approx A \beta_h(0) \beta_N(0), \tag{4.11}$$

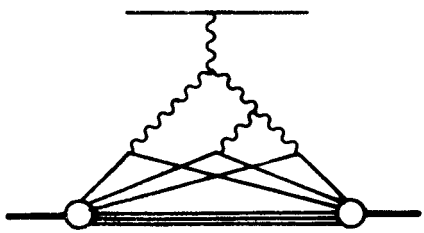

Fig. 30. Dominant diagrams for $\alpha_P(0) \approx 1$, $g_{PPP}(0) \neq 0$ and $A^{1/3} \ln s$ large

we see that it can be quite significant for $A^{1/3} \ln s$ large[20]. The dominant diagrams are the n the "fan diagrams" [22] shown in Fig. 30. It is amussing that these can be explicitly su mmed to give [23]

$$\sigma \approx A \beta_h(0) \beta_N(0) \Big/ \left(1 + \frac{A^{1/3} \beta_N(0) g_{PPP}(0)}{16\pi^2 R_0^2} Y\right), \tag{4.12}$$

---

[19] We have rotated the M^2 contour freely. The corrections discussed at the end of Section 3 are negligible to leading order in ln s here.

[20] We consider the regime $|\alpha_P(0) - 1| \ln s \ll 1$ so the pole and cut terms have the same energy dependence.

where we have neglected ln AmR compared to Y for simplicity. Equations (4.11) and (4.10) are the first two terms in the series expansion of (4.12). A similar expression holds for the single-particle inclusive cross-section in the central region

$$\left.\frac{d\sigma}{dy}\right|_A = \left.\frac{d\sigma}{dy}\right|_N A \Big/ \left(1 + \frac{A^{1/3}\beta_N(0) g_{PPP}(0)}{16\pi^2 R_0^2}\, y\right). \tag{4.13}$$

It is important to note that y and not Y appears in (4.13), since due to the AGK cancellation effect all fans starting at rapidities greater than y give vanishing contribution to $d\sigma/dy$.

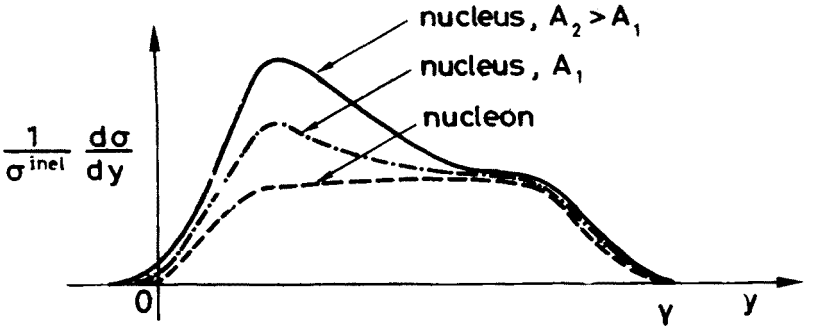

Fig. 31. Single-particle spectra for $\alpha_P(0) \approx 1$ and $g_{PPP}(0)\, A^{1/3}\ Y$ large

The inclusive cross-section thus has the form shown in Fig. 31. There is no plateau for large A!

The above examples show that the behaviour of the inclusive cross-section is quite dependent on the actual values of the parameters in hadron-hadron scattering. We shall find in the next section where we turn to phenomenology that neither of the above examples is relevant at present energies.

5. *Phenomenological implications*

We now discuss briefly the phenomenological implications of the Regge model for hadron-nucleus collisions for current energies ($p \lesssim 10^4$ GeV/c) and available nuclei ($A \lesssim 250$). We begin with a review of hadron-hadron phenomenology.

5.1. Hadron-hadron phenomenology

We follow the work of Capella, Kaplan and Tran [26] and Capella and Kaidalov [27]. These authors take $\alpha_P(0) \gtrsim 1$ and $g_{PPP}(0) \neq 0$. From an analysis of the proton-proton cross-section at a given energy (say ln $s = 5$) they have

$$(\beta_p(0))^2 \approx 62 \text{ mb} \approx 160 \text{ GeV}^{-2},$$

$$2\gamma_p \approx 3.3 \text{ GeV}^{-2}. \tag{5.1}$$

Single Pomeron exchange alone thus gives a σ_{pp}^{tot} of 62 mb; multiple Pomeron exchanges (Fig. 32a) reduce this to the observed 43 mb. The contribution of n-Pomeron exchange can be expressed as a multiple dispersion integral over the multiple discontinuity of the blobs in the variables M_i^2 just as in Eq. (2.25). First consider the contribution of just

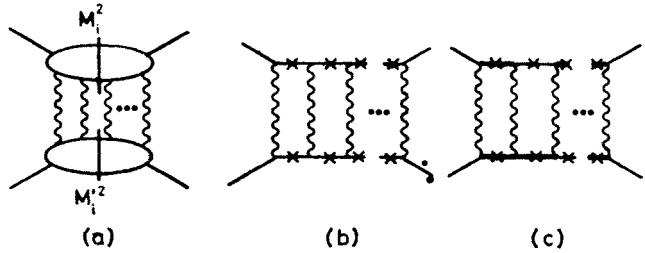

Fig. 32. a) n-Pomeron exchange contribution to elastic amplitude. b) Elastic contribution only. c) Elastic and resonance contributions

the elastic state in each M_i^2 (Fig. 32b). The sum of all such terms has the eikonal form

$$\mathscr{A}(s,0) = \mathscr{A}^{(1)}(s,0) \sum_{n=1}^{\infty} \left(\frac{i\mathscr{A}^{(1)}(s,0)}{8\pi(2\gamma_p\alpha' \ln s)s} \right)^{n-1} \frac{1}{nn!} \equiv \mathscr{A}^{(1)}(s,0) \sum_{n=1}^{\infty} \left(-\frac{z}{2} \right)^{n-1} \frac{1}{nn!} \tag{5.2}$$

From (5.1) we have $z = 2.33$. For such a large value of z, the multiple Pomeron exchanges are quite important — the two-Pomeron exchange being $\approx 30\%$ of the one-Pomeron exchange, for example. The contribution of low mass N* resonances (Fig. 32c) can be taken into account by a straightforward generalization of (5.2). Using results on single diffractive production of resonances, they estimate

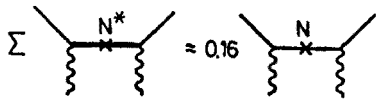

(5.3)

This means the total two-Pomeron contribution is approximately $(1.16)^2 \approx 1.3$ times the purely elastic contributions. Assuming the N* couplings to the Pomeron equal the proton coupling, one can compute the graphs of Figs 32b and c to obtain $\sigma^{(1)} = 62$ mb, $\sigma^{(2)} = -25$ mb, $\sigma^{(3)} = 10$ mb, $\sigma^{(4)} = -4$ mb, $\sigma^{(5)} = 1$ mb, $\sigma^{(6)} = -0.4$ mb, and $\sigma^{tot} = 43$ mb.

The blobs in Fig. 32a also contain contributions from high mass non-resonant diffractively produced states. Thus the M^2 discontinuity of the Pomeron-particle amplitude of Fig.12 has the behaviour shown in Fig. 33. For $M^2 < \Lambda = 5\,\text{GeV}^2$ the contribution is well approximated by the elastic and resonance contributions, while for $M^2 > \Lambda$ it is

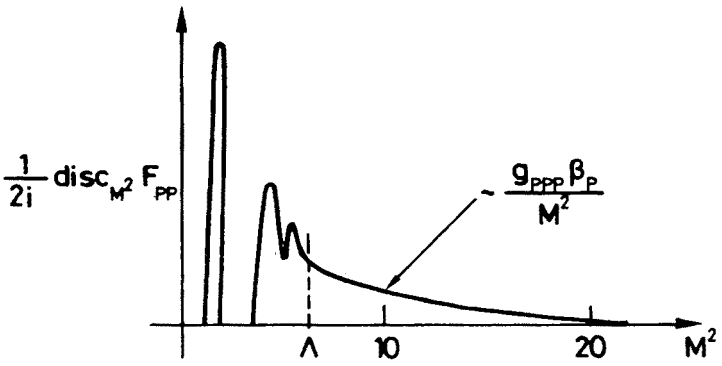

Fig. 33. Imaginary part of the Pomeron-proton amplitude

well approximated by the triple-Pomeron. Therefore the contribution of large M^2 in the upper blob is given by an expression similar to Eq. (4.9)

$$\sigma^{(Y)} = -\frac{1}{s}\int \frac{d^3q}{(2\pi)^3}\,\frac{1}{2m}\,\mathrm{disc}_{M^2} V^{(2)}\beta_N^2(\vec{q}^{\,2})$$

$$= -\frac{1}{16\pi^2}\int dt \int d\frac{M^2}{s}\left(\frac{M^2}{s}\right)^{\alpha(0)-2\alpha(t)} \beta(0) g_{PPP}(t)\beta^2(t), \tag{5.4}$$

where we have included only the elastic state in the lower blob. The triple-Pomeron coupling is obtained from inclusive cross-section measurements for $M^2/s \lesssim 0.1$,

$$\frac{d\sigma}{d\dfrac{M^2}{s}\,dt} = \frac{1}{16\pi^2}\,\beta(0) g_{PPP}(t)\beta^2(t)\left(\frac{s}{M^2}\right)^{2\alpha(t)}\left(\frac{M^2}{s}\right)^{\alpha(0)} \equiv G(t)\left(\frac{M^2}{s}\right)^{-1-2\alpha' t} \tag{5.5}$$

with $G(t) \approx (2.5\ \mathrm{mb} - \mathrm{GeV}^{-2})\, e^{(2\gamma p+\gamma)t}$, where $\gamma = 1\ \mathrm{GeV}^{-2}$. Substituting (5.5) in (5.4) we have

$$\sigma^{(Y)} \approx -\int_{\Lambda/s}^{0.1} d\frac{M^2}{s}\left(\frac{M^2}{s}\right)^{-1} \frac{1}{2\gamma p+\gamma+2\alpha' \ln\dfrac{s}{M^2}}\, G(0)$$

$$\approx \frac{2.5\ \mathrm{mb\ GeV}^{-2}}{5.5\ \mathrm{GeV}^{-2}} \ln\frac{0.1}{5/s} \approx -0.5\ \mathrm{mb} \ln\frac{s}{50} \approx -2\ \mathrm{mb}. \tag{5.6}$$

The total contribution will be modified somewhat by elastic and inelastic rescattering analogous to Figs 32b and c, but Eq. (5.6) indicates that the "Y-graph" contribution is rather small[21].

[21] It must be noted, however, that the quantity $G(t)$ extracted from inclusive cross-sections (5.5) may differ significantly from the bare triple-Pomeron coupling due to the presence of absorptive corrections [28].

Graphs containing several large M_i^2 contributions lead to "Reggeon loops" such as shown in Fig. 34. These are smaller than the corresponding pole terms by a factor [26, 29]

$$\frac{g_{PPP}(0)}{8\pi^3\alpha'} \ln s \sim 10^{-2} \ln s \tag{5.7}$$

and are therefore negligible.

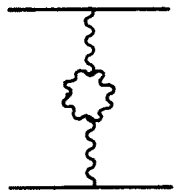

Fig. 34. Simplest Reggeon-loop graph

We now discuss briefly the energy dependence of σ_{tot}. For $\alpha(0) = 1$, the graphs of Fig. 32 increase only slightly ($\approx$ 2mb) over the ISR energy range if they are evaluated treating s as asymptotic. The Y-graphs give a negative contribution which increases in magnitude with energy. Hence the total cross-section is rather constant or perhaps even decreasing with energy. To obtain the observed increase of the cross-section one must take $\alpha(0) \approx 1.1$ [26]. The renormalized (by graphs like Fig. 34) Pomeron intercept is also greater than one due to the smallness of (5.7) and the Froissart bound is enforced by the graphs of Fig. 32 [22].

Recently, it has been pointed out that s cannot really be treated as asymptotic in the evaluation of the multi-Regge exchange graphs [27]. Consider, for example, the imaginary part of the two-Regge exchange graph which has three contributions like those shown in Figs 13 and 14. The contribution with a cut through both Reggeons presumably has a higher threshold than the other terms since the energy is shared between two multiperipheral chains. Thus at non-asymptotic energies the weight of this term may be less than the usual +2 with the result that the graph is larger in magnitude. These kinematic effects will then tend to reduce the cross-section at lower energies giving a marked rise of the contribution of graphs of the form of Fig. 32. With a reasonable ansatz for the kinematic effects, Capella and Kaidalov could reproduce the observed rise of the cross-section with $\alpha(0) = 1$ [23].

Actually, most of the qualitative implications of hadron-hadron phenomenology for hadron-nucleus scattering that we will discuss do not depend much on the values (5.1). For example, one could use the pre-ISR phenomenology where σ^{tot} asymptotes to 40 mb, or the work of the Leningrad group [33] who take $g_{PPP}(0) = 0$. The crucial aspect is the smallness of the triple-Pomeron coupling.

---

[22] The theoretical acceptability of such a scheme is presently under debate. It is not clear that the renormalized intercept can ever be above unity [30].

[23] Or $\alpha(0)$ equal to the critical value (slightly greater than one) for which the renormalized intercept is exactly one. For other discussions of such kinematic effects, see Refs [31] and [32].

5.2. Hadron-nucleus phenomenology

We first consider the energy and A dependence of the total cross-section. For relatively low energies $p \ll m^2R$ the M^2 values in (3.6) are restricted to $M^2 \approx m_h^2$ and the elastic Glauber formula is expected to hold to good approximation, We can use Eq. (2.32) for large A. Absorption is very large for big nuclei and we can be near the black disk limit

$$\sigma^{el} \approx \sigma^{inel} \approx \pi R^2. \tag{5.8}$$

At higher energies, low mass diffractive production becomes important and this leads to further absorption and decrease of the cross-section for $p \approx M^2R$. This behaviour is observed and Glauber fits with inelastic rescattering are in adequate agreement with the data [34].

At very high energies, graphs containing the triple-Pomeron vertex (for example, Fig. 26e) will become important and the Glauber formula will no longer hold. This will occur, roughly speaking, when Figs 26 e and 26c comparable [15].

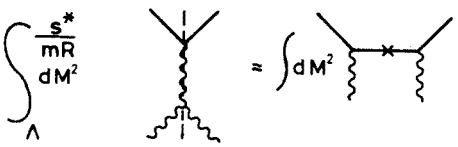

(5.9)

i.e.

$$\frac{1}{16\pi^2}\beta^3(0)g_{PPP}(0)\ln\frac{s^*}{\Lambda mR} \approx \frac{\pi\beta^4(0)}{19\pi^2}.$$

This gives

$$\ln\frac{s^*}{25A^{1/3}} \approx 70. \tag{5.10}$$

Although the precise value is strongly dependent on $\beta(0)$, it is fairly clear from such estimates that triple-Pomeron interactions are important at only extremely high energies. Indeed the energies are comparable with those at which Pomeron loops (Fig. 34) are important and thus a treatment involves the solution of the full Reggeon field theory (see, for example, Ref. [6]).

It is also important to make some estimate of the Pomeron residue renormalization (see Eq. (3.14)). If it is important there will be significant effects for the single-particle inclusive cross-section in the central region since it is proportional to β_A (Fig. 28). The lowest order term is Fig. 26a, and is given by (4.11), while the triple-Pomeron contribution is given by (4.10) (see, however, footnote 15). The ratio is thus

$$\frac{\beta_A^{(2)(PPP)}}{\beta_A^{(1)}} \approx \frac{A^{1/3}G_{PPP}}{\beta^2(0)R_0^2}\ln\frac{s^*}{\Lambda mR} \approx -\frac{A^{1/3}}{600}\ln\frac{s^*}{25A^{1/3}}. \tag{5.11}$$

An estimate of the Reggeon-Reggeon-Pomeron triple coupling can be obtained from Eq. (3.24) with the result

$$\frac{\beta_A^{(2)\,(\mathrm{RRP})}}{\beta_A^{(1)}} - \approx \frac{2G_{\mathrm{RRP}}}{R_0^3\beta^2 m} \ln \varepsilon mR \approx \frac{\ln 5A^{1/3}}{125}, \tag{5.12}$$

where we used $G_{\mathrm{RRP}} = 30$ mb/GeV^{-2} [35]. Both contributions are very small. All such estimates must be treated with great caution, however. As we emphasized in Section 3, the nuclear structure enters in a non-trivial way. Although they are suppressed, contributions for $M^2 \geqslant p/R$ do give contributions as (5.11) shows. We can have contributions for

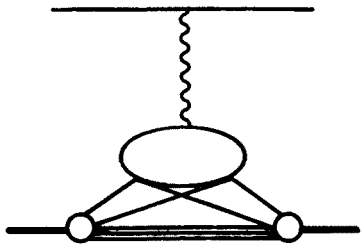

Fig. 35. Diagram appropriate for $M^2 \approx s^*$

$M^2 \approx s^*$ for which one must use the more general couplings of Fig. 35. Also as one can see clearly from (3.25) one needs a knowledge of the full six-particle hadronic amplitude and not only its M^2 discontinuity[24]. Nonetheless, since the discontinuity of the amplitude for the $M^2 \approx s^*$ region is expected to be related to the $M^2 \ll s^*$ region by duality and the full amplitude is closely related to its discontinuity through analyticity, one might expect that (5.11) and (5.12) give order of magnitude estimates. Therefore, in the absence of evidence to the contrary, I shall assume the Pomeron residue renormalization is small in the following.

It should be emphasized that this is a very different position from that advocated by Koplik and Mueller [16]. They argue on general grounds that in "soft field theory" (which leads to Regge behaviour — see Appendix) Regge residue renormalization must be important for large A so that $\beta_A \propto A^{2/3}$. When this is the case the single and multiple Regge exchange contributions to the elastic amplitude each receive contributions from a large number of multiple scattering terms $A_{hA}^{(n)}$. The multiple scattering expansion (2.1) is then not very useful and the natural expansion is in terms of the number of Regge exchanges, each with fully renormalized residue. Since the actual values of the renormalized residues depend upon detailed dynamics, it is difficult to obtain quantitative results for cross sections, multiplicities, etc. in this case. (Koplik and Mueller have obtained some general relationships, however. These are qualitatively similar to those discussed in the following paragraph.) It is similarly difficult to estimate for what values of A the large A behaviour sets in and thus to know if it is applicable to available nuclei. Although the estimates given in the above paragraph would indicate that it is not applicable, they must

[24] This point has been emphasized by several authors; see, for example, Refs [16] and [32].

be treated with very great caution and it is possible that Regge residue renormalization is important for available nuclei. This question is central to the Regge description of hadron--nucleus scattering and needs further study.

I thank A. Mueller for very informative discussions on these points.

We turn to single-particle inclusive cross-sections. The central region is simplest to discuss. Owing to the AGK cancellation mechanism only the simple Mueller diagram of Fig. 28 contributes (neglecting diagrams of the form of Fig. 23 as usual). On the basis of the arguments given above, the nuclear vertex is $A\beta_N$ so

$$\frac{d\sigma_{hA}}{dy} \sim \beta_h(0) G^{h_3} A \beta_N s^{\alpha(0)-1}. \tag{5.13}$$

We have then

$$\frac{1}{\sigma_{hA}^{inel}} \frac{d\sigma_{hA}}{dy}\bigg|_{central} = \bar{\nu} \frac{1}{\sigma_{hN}^{inel}} \frac{d\sigma_{hN}}{dy}\bigg|_{central}, \tag{5.14}$$

where $\bar{\nu}$ is the average number of interactions defined by

$$\bar{\nu} = \frac{A\sigma_{hN}^{ihel}}{\sigma_{hA}^{inel}}. \tag{5.15}$$

Since $\sigma_{hA}^{inel} \approx \pi R^2 \alpha A^{2/3}$ we have the central region growing approximately as $A^{1/3}$ [16, 36] which is quite different from that discussed in either of the examples considered in Section 4[25]. Thus, as a result of the AGK cancellation, if the total cross-section approaches the black disk limit, the inclusive cross-section must grow roughly as $A^{1/3}$ in the central region [16, 36].

In the projectile fragmentation region the situation is rather more complicated due to the presence of multi-Regge exchanges (Fig. 28). These are quite important even in hadron-hadron scattering (diffraction dissociation comes only from diagrams with $n \geqslant 2$ and is sizeable) and can be only more important in the nuclear case due to the enhancement of diagrams with large n. Since the n-fold rescattering diagram contains contributions with cuts through $k \leqslant n$ Pomerons (which have k times the usual density of particles), we might naïvely expect a large A-dependence of $d\sigma/dy$. However, it has recently been pointed out [27] that one does not expect cuts through more than one Pomeron to contribute near the phase space boundary. For example, if one supposes that the cut through two Pomerons is initiated by the splitting of a given particle into two virtual constituents (as in Fig. 14c) and each of these has half the incident momentum, this cut contributes only up to $y = Y - \ln 2$. Thus the shape of the non-diffractive part of the fragmentation spectrum should be A independent for $y > Y - \ln 2$. However, these arguments are not sufficient to exclude A dependence of $1/\sigma^{inel}\, d\sigma/dy$ in the leading part of the fragmentation region since there are absorptive effects in $d\sigma/dy$ and σ^{inel} includes contributions from cuts through any number of Pomerons. Both of these are A-dependent. Stated

[25] We re-emphasize that this depends on nuclear Regge residue renormalization being negligible.

another way, while the energy-momentum sum rule

$$\int dy e^{y-Y}\left(\sum_{h_3}\int d^2p_\perp \frac{\mu_{h_3}}{m_h}\frac{1}{\sigma_{hA}^{inel}}\frac{d\sigma_{hA}^{inel,\,h_3}}{d^2p_\perp dy}\right)=1 \tag{5.16}$$

constrains the single-particle spectrum, the contribution of the cut through one Pomeron could be either somewhat reduced or increased with the excess or deficit of energy being carried off either by slower particles arising from the cuts through several Pomerons or by diffractively produced particles.

We are able to say little about the nuclear fragmentation region for the reasons discussed below Eq. (5.12). Energy momentum conservation will constrain the spectrum somewhat, but its consequences will be weaker since the nucleons carry most of the momentum and energy. In Fig. 36 we sketch the single-particle inclusive spectrum to be expected on the basis of the above discussion[26]. According to Ref. [27], the central region behaviour (Eq. (5.15)) only obtains when the rapidity differs from Y by more than $\ln 2\bar{\nu}$, since the

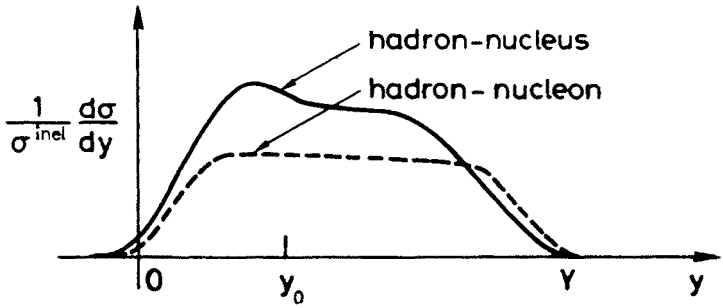

Fig. 36. Single-particle inclusive spectra

AGK rules only hold when energy-momentum conservation effects are unimportant (all discontinuities through the average number ($\bar{\nu} \propto A^{1/3}$) Pomerons are unaffected). Owing to this effect in the central region $dn/dy|_A/dn/dy|_N$ will increase with energy to $\bar{\nu}$ (for energies below those for which triple Pomeron interactions become important). As we move towards $y = Y$ we expect a dependence on A weaker than $A^{1/3}$ since cuts through fewer and fewer Pomerons are allowed. A more detailed study of the model with the implementation of energy momentum conservation is necessary before it will be clear whether these behaviours are consistent with the data (see, for example, Ref. [37]). The central region behaviour may provide a very critical test of the model.

We have discussed above only the qualitative features of the simplest inclusive processes with emphasis on the A and s dependence. Even these await quantitative confrontation with experiment. However, hadron-nucleus collisions offer us a great wealth of other information which the theory should explain. Some of these which are most directly related to the theory are fluctuations in the multiplicity distribution [32], two-particle correlations outside the nucleus fragmentation region, and correlations between the number of knocked-out nucleons (N_h for emulsions) and the total multiplicity[27]

[26] Diffractively produced particles have been excluded. They require a separate discussion.

[27] For some calculations within the model of Schwimmer [25], see the second reference of Ref. [25].

and rapidity distributions. As far as the latter point is concerned, since contributions with N-struck nucleons only arise from cuts through N Reggeons we expect the multiplicity to be proportional to N_h since empirically N_h is proportional to N. Since the diagram of Fig. 32c dominate and cuts through fewer and fewer ladders contribute to dn/dy as $y \to Y$, we expect the coefficient of N_h in $dn/dy = d\alpha/dy + (d\beta/dy)N_h$ to decrease to zero as $y \to Y$, so dn/dy becomes less than that for hydrogen for large N_h. At least qualitatively one sees that N_h can be used as a measure of the number of cut ladders. In hadron-hadron collisions we have no such probe available. This is just one way in which hadron-nucleus collisions can be used to test the model in more subtle ways than is possible in elementary particle reactions.

Above we have discussed only the case of large A. Interesting information can also be obtained from small nuclei. Let us consider the deuteron. In this case, a formula like (3.2) but in terms of the deuteron form factor can be derived without use of the approximation (2.26) [4]. Thus the cross-section deficit

$$\delta\sigma_{\pi^-d} = \sigma^{\text{tot}}_{\pi^-p} + \sigma^{\text{tot}}_{\pi^-n} - \sigma^{\text{tot}}_{\pi^-d} = -\frac{1}{s}\,\text{Im}\,A^{(2)}_{\pi^-d} \tag{5.17}$$

can be calculated explicitly. Since $\delta\sigma$ can be directly measured, we can measure a small term which we could not measure for a large nucleus. The dominant contribution to $\delta\sigma$ is the elastic pion pole ($\approx$ 1.4 mb) as expected from our previous discussions. According to the most recent and thorough evaluation [38], the next most important term is the triple-Pomeron which grows like $0.2 \ln p$ mb and thus manifests itself by a significant logarithmic increase in $\delta\sigma$ [28]. One can anticipate using the deuteron as a testing ground for other properties of the model.

I would like to thank H. Lubatti for stimulating my interest in hadron-nucleus scattering. I am greatly indebted to M. Baker for many discussions on the subject which generated not only enlightenment but also enthusiasm. I would like to thank G. Winbow for several very informative discussions and L. Bertocchi and A. Capella for many helpful discussions on the material in Section 5. I also thank R. C. Brower, R. N. Cahn, S. Ellis, T. Jaroszewicz, H. Kühn, J. Miller, A. Mueller, A. R. White and K. Zalewski for very useful discussions. I thank D. Amati for the hospitality of the CERN Theory Division.

APPENDIX

Physical space-time picture of Regge exchange

We briefly discuss the physical space-time picture of Regge exchange in the multiperipheral model. For further discussion we refer the reader to Refs [4, 16, 19], and [39].

In the multiperipheral model the fundamental high-energy interaction between two hadrons occurs through production processes of the form shown in Fig. 5a, where n

[28] This work was based on approximately constant hadron cross-sections. Since πN cross-sections actually are increasing there will be other increasing terms which will tend to obscure the triple-Pomeron contribution to an increase in $\delta\sigma$.

is large since the amplitude is assumed to be small when any of the subenergies $(p_i+p_j)^2$ is large. Two further important characteristics of the model are the rapid decrease of amplitudes for large t_i and the absence of correlations between particles widely separated in Fig. 5a. Although these very general properties of "soft field theory" are sufficient to allow us to derive all the results discussed below [6, 16, 19] we will discuss for concreteness the explicit realization of the model in terms of ladder graphs in ϕ^3 field theory [40]. We develop a space-time picture for the model by studying old-fashioned perturbation theory.

Consider the process of Fig. 5a. The momenta p_i are ordered so that the momentum transfers are small. It can be shown[29] that in the laboratory frame (Eq. 1.14))

$$|p_{iT}| \approx \mu, \tag{A.1}$$

where μ is the mass in the theory and

$$p_{h_1 z} \equiv p_z \geqslant p_{1z} \geqslant p_{2z} \geqslant p_{3z} \geqslant \cdots,$$

where the inequalities extend down to $|p_{iz}| \approx \mu$. Furthermore, typically one has

$$Q_{iz} = Q_{i-1,z} - p_{iz} \approx C^{-1} Q_{i-1,z} \approx \tfrac{1}{2} Q_{i-1,z}. \tag{A.2}$$

We consider first the old-fashioned perturbation theory graph shown in Fig. 37[30], and discuss the time ordering

$$t_1 < t_2 < t_3 < \ldots < t_n \tag{A.3}$$

for which the amplitude is given by

$$iA(2\pi)^4 \delta^4(p_{h_1}+p_{h_2}-\sum_{i=1}^{n} p_i) = (-i)^n \int_{-\infty}^{\infty} dt_n \int_{-\infty}^{t_n} dt_{n-1} \ldots \int_{-\infty}^{t_2} dt_1 H_I(t_n) \ldots H_I(t_1), \tag{A.4}$$

where

$$H_I(t) = \int d^3x H_I(x) = \int d^3x g\phi^3(x) \tag{A.5}$$

and

$$\phi(x) = \frac{1}{(2\pi)^{3/2}} \int \frac{d^3p}{\sqrt{2E_p}} (a(p)e^{-ip\cdot x} + a^+(p)e^{ip\cdot x}). \tag{A.6}$$

A vertex like that shown in Fig. 38a gives a factor

$$\int_{-\infty}^{t} dt' H_I(t') \propto \frac{e^{-i(E_i-E_j-E_k)}}{E_i-E_j-E_k} \delta^3(\vec{p}_i-\vec{p}_j-\vec{p}_k). \tag{A.7}$$

The denominator in (A.7) means that times t' of the order $\tau \approx |E_i-E_j-E_k|^{-1}$ are important

[29] See, for example, Chapter Ic of Ref. [6].

[30] Graphs with other orderings of the p_l are smaller because they involve larger subenergies $(p_i+p^j)^2$.

in the integral. If the momenta are small $|p_{l,\alpha}| \approx \mu$ where μ is the mass in the theory, then

$$\tau \approx \frac{1}{\mu} \quad (|p_l| \approx \mu), \tag{A.8}$$

which gives the basic time scale of the interaction.

In Fig. 37 there are vertices involving momenta with large z-components so that

$$E_l \approx |p_{l,z}| + \frac{p_{lT}^2 + \mu^2}{2|p_{l,z}|}. \tag{A.9}$$

Then

$$E_i - E_j - E_k \approx |p_{iz}| - |p_{jz}| - |p_{kz}| + \frac{\mu^2}{p_{lz}} \approx \frac{\mu^2}{p_{lz}} \tag{A.10}$$

since from (A.2) all the momenta entering the vertex have the same sign and are of the same order of magnitude. We then have

$$\tau \approx \frac{p_{lz}}{\mu} \quad (|p_{lz}| \gg \mu), \tag{A.11}$$

which is recognized as the boosted version of (A.8). Fixing $t_n = 0$ (the integral over t_n

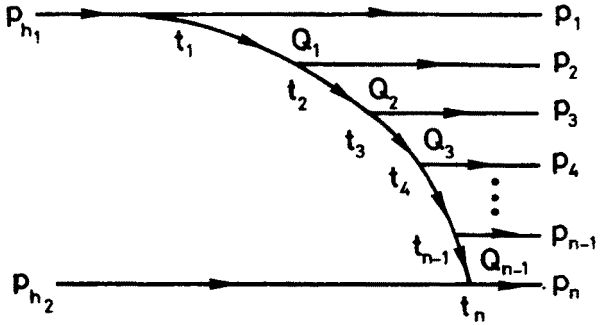

Fig. 37. Old-fashioned perturbation theory graph for production process

gives energy conservation), we see that the l-th interaction in Fig. 37 takes place at a time of order

$$t_l \approx -(C^{-1})^{l-1} \frac{p_z}{\mu^2}. \tag{A.12}$$

For other time orderings there occur vertices of the type shown in Fig. 38b. These give a factor $(E_i + E_j + E_k)^{-1} \approx p_z^{-1}$ and therefore smaller by a factor p_z^{-2} in the high-energy limit.

The physical picture of the multiperipheral model in longitudinal space and time can therefore be described as follows: At a long time ($\approx p_z/\mu^2$) and distance before reaching the target, the fast incident particle emits a particle of momentum p_1, reducing its momen-

tum to $C^{-1}p_z$. Later, at a time $\approx C^{-1}p_z/\mu^2$ before reaching the target, it emits a second particle reducing its momentum to $C^{-2}p_z$. Only after emitting a large number of particles so its energy is of order μ does it finally interact with the target[31]. To undergo a scattering,

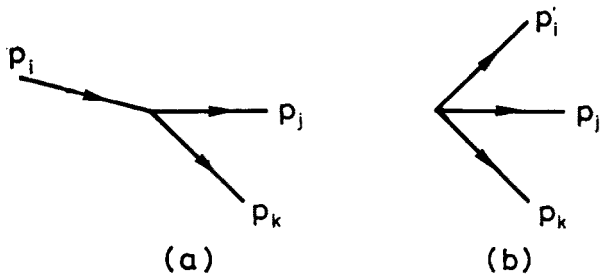

Fig. 38. Interactions occurring in a) dominant and b) suppressed time orderings

the projectile must start emitting particles[32] at distances $\approx p_z/\mu^2$ before reaching the target! The basic Regge exchange process (Fig. 1) occurs over a very large distance $\approx p_z'/\mu^2$ in the laboratory at high energies — see Fig. 39.

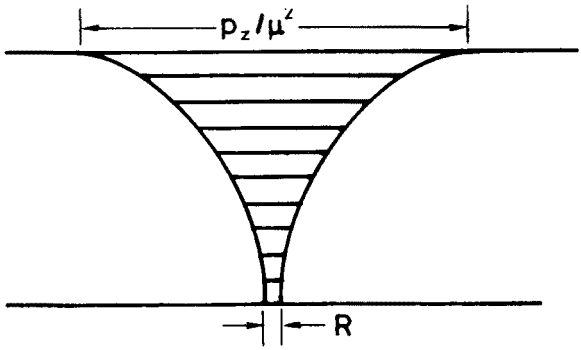

Fig. 39. Spatial development in elastic scattering by single Regge exchange. R is the dimension of the target

The multiperipheral model also has an interesting physical picture in transverse space [4], but since this is not essential to what follows, we will not discuss it here. We turn instead to some applications involving multiple Regge exchange processes.

It is now trivial to see the famous vanishing of the AFS graph (Fig. 17a) at high energies — see Fig. 40. Since z_0 must be of order of the size R of the target the graph vanishes for

$$\frac{2p_z}{\mu^2} \gg R. \tag{A.13}$$

This is in complete agreement with the discussion of Section 3, where we found that when

[31] Note $(C^{-1})^{n-1}\, p_z \approx \mu$ implies the well-known result $n \approx (1/\ln c) \ln s + b$.

[32] These are, of course, virtual until the interaction with the target which allows energy conservation has taken place.

(A.13) was satisfied, the cut Regge contribution could be expressed in terms of the fixed pole residue (3.15). The latter vanishes for the AFS diagram.

On the other hand, the Mandelstam graph is perfectly acceptable from a space-time point of view — see Fig. 41. The space-time picture for this graph is quite helpful since it can be used to give a relatively simple derivation of the AGK rules (at least for $R > 1/\mu$) [19].

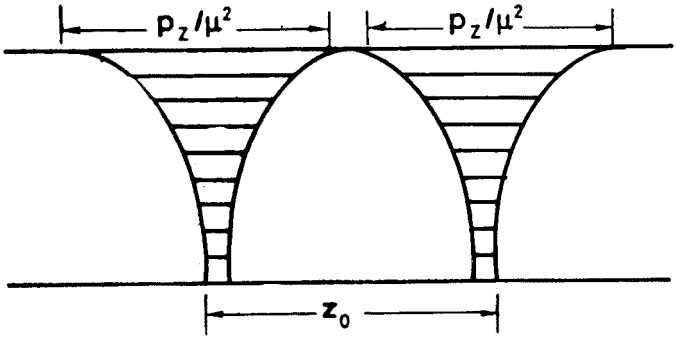

Fig. 40. Spatial development of the AFS graph

We now return to hadron-nucleus scattering. We can imagine the incident hadron before it reaches the nucleus developing virtual states like those shown in Fig. 42. In addition to the basic single chain, there are various multiple chain states. After interaction with the target nucleus, we therefore have final states with different distributions of particles.

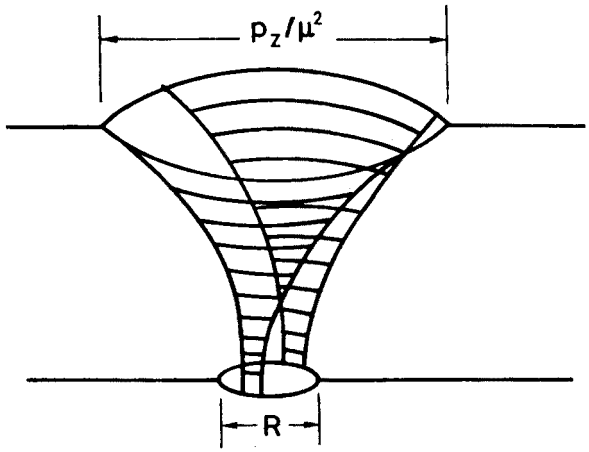

Fig. 41. Spatial development of the Mandelstam graph

Since the probability of each chain interacting with the nucleus is proportional to $A^{1/3}$ [33] we would expect generally a different distribution of final states for each A.

Let us return for a moment to the (unrealistic) example of $\alpha_P(0) < 1$ discussed at the end of Section 4. The contributions of the double chain states (Figs 42b, c, and d)

[33] For $p' \lesssim \mu^2 R$, the probability is less than this because the lifetime of the virtual particle is shorter than the time it takes it to traverse the nucleus [16].

is not a priori negligible due to the $A^{1/3}$ enhancement, and has the behaviour as a function of p' shown in Fig. 20. Furthermore, AFS-like graphs (Fig. 42d) can contribute for a much larger range ($p' \leqslant \mu^2 R$) than they do in hadron-hadron scattering. The nuclear dependence of the interaction thus extends over produced particles of rapidities $y \lesssim y_0$ (Eq. 4.7)). If we consider the single-particle inclusive cross-section we see that the contributions of Mandelstam-like graphs (Figs 42b and c) cancel each other for $y \geqslant y_0$ (see also Fig. 22). For $y \lesssim y_0$ all the multiple chain states may contribute giving Fig. 29. The situation can be described by saying that for $p' \gtrsim \mu^2 R$, the lifetime of the virtual particles is long and

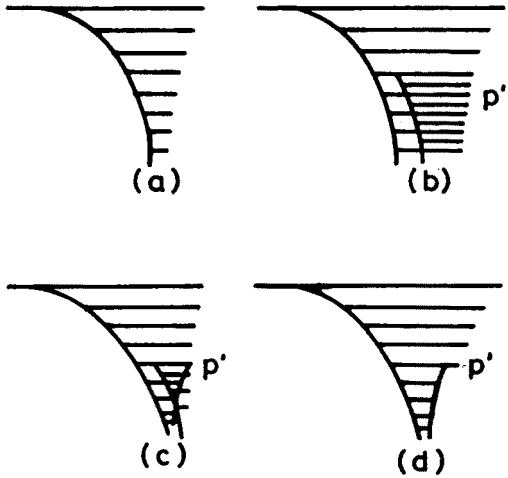

Fig. 42. Virtual states of incident hadron corresponding to a) single Regge exchange, b) and c) Mandelstam--like triple-Regge contributions, and d) AFS-like triple-Regge contribution

the nucleus is transparent to them (owing to the "softness" of the theory) while for $p' \leqslant \mu^2 R$ the lifetime is less than the nuclear size and sequential scatterings can take place. However, it must be recalled that the suppression of the many chain states only occurs for $\alpha_P(0) < 1$ and $|1-\alpha_P\ (0)| \ln p' \gg 1$.

It should be remarked that the break-up into AFS-like and Mandelstam-like graphs and their different properties, which is immediate in this picture, is not a new feature of the problem which we have overlooked in the main body of the text. It is no more than a particular aspect of the phenomena that the amplitude for $p' \lesssim \mu^2 R$ cannot be expressed completely in terms of the discontinuity of the Reggeon-particle amplitude. Therefore, Feynman graphs like the AFS graph which have vanishing integrals over their discontinuities can contribute. I do not feel that the decomposition of the contribution into separate Mandelstam and AFS parts has much significance or utility. It is better to deal directly with the expressions of Section 3 in which the Reggeon particle amplitude is treated generally using dispersion relations and analyticity instead of being treated as a sum of particular Feynman graphs.

For $\alpha_P(0) \gtrsim 1$, the many chain states no longer decrease with energy and they can give important contributions for all values of the produced particles. The simplicity of

the picture of Figs 37 or 42a is then lost. It thus appears that the space-time picture in the multiperipheral model, which has great appeal from and intuitive physical point of view, gives us a simple picture for hadron-nucleus scattering only for $\alpha_P(0) < 1$. In this case there is also a close correspondence to the parton model (see, for example, Refs [16] and [39]), so one can equivalently use the parton picture although further elaboration of the hadron-hadron model is necessary to discuss the interaction of the "wee" partons with the nucleus. I believe the correct elaboration is just that abstracted from the Regge model[34]. For the bare Pomeron intercept $\alpha_P(0) > 1$, the space-time picture is not too useful and furthermore the parton model probably cannot be formulated[35]. Unfortunately, it appears that this is the actual situation.

Editorial note. This article was proofread by the editors only, not by the author.

REFERENCES

[1] P. D. B. Collins, E. J. Squires, *Regge Poles in Particle Physics*, Springer-Verlag, Berlin 1968; P. D. B. Collins, *Phys. Rep.* **1C**, 103 (1971).

[2] R. J. Glauber, in *High Energy Physics and Nuclear Structure*, North Holland, ed. G. Alexander, Amsterdam 1967, p. 311.

[3] M. Gell-Mann, B. M. Udgaonkar, *Phys. Rev. Lett.* **8**, 346 (1962).

[4] V. N. Gribov, *Zh. Eksp. Teor. Fiz.* **56**, 892 (1969) (English translation. *Sov. Phys. JETP* **29**, 483 (1969)); *Yad. Fiz.* **9**, 640 (1969) (English translation: *Sov. J. Nucl. Phys.* **9**, 369 (1969)).

[5] E. S. Abers, H. Burkhardt, V. L. Teplitz, C. Wilkin, *Nuovo Cimento* **42**, 365 (1966); P. V. Landshoff, *Phys. Rev.* **177**, 2531 (1969).

[6] M. Baher, K. A. Ter-Martirosyan, *Phys. Rep.* (to be published).

[7] V. N. Gribov, *Zh. Eksp. Teor. Fiz.* **57**, 709 (1969) (English translation: *Sov. Phys. JETP* **30**, 709 (1970).

[8] L. Bertocchi, *Nuovo Cimento* **11A**, 45 (1972).

[9] J. D. Bjorken, S. D. Drell, *Relativistic Quantum Fields*, McGraw-Hill, New York 1965.

[10] V. N. Gribov, *Zh. Eksp. Teor. Fiz.* **53**, 654 (1967) (English translation: *Sov. Phys. JETP* **76**, 414 (1968)).

[11] R. C. Brower, C. E. DeTar, J. H. Weis, *Phys. Rep.* **14C**, 257 (1974).

[12] I. J. Muzinich, F. E. Paige, T. L. Trueman, L.-L. Wang, *Phys. Rev*, **D6**, 1048 (1972).

[13] S. Mandelstam, *Nuovo Cimento* **30**, 1127 (1963); **30**, 1148 (1963).

[14] I. G. Halliday, C. T. Sachrajda, *Phys. Rev.* **D8**, 3598 (1973).

[15] G. A. Winbow, Rutgers reports (1976).

[16] J. Koplik, A. H. Mueller, *Phys. Rev*, **D12**, 3638 (1975).

[17] V. A. Abramovskii, V. N. Gribov, O. V. Kancheli, *Yad. Fiz.* **18**, 585 (1973) (*Sov. J. Nucl. Phys.* **18**, 308 (1974)).

[[18] M. Baker, L. D. McLerran, Report at Internat. Conf. on High-Energy Physics, Palermo 1975.

[19] J. Koplik. A. H. Mueller, *Phys. Lett.* **58B**, 166 (1975).

[20] L. D. McLerran, J. H. Weiss, *Nucl. Phys.* **B100**, 329 (1975).

[21] J. H. Weiss, University of Washington Report RLO-1388-711 (1976).

[34] This point of view has also been advocated in Ref. [41]. For an extensive discussion of the parton model, but with a different point of view, see Ref. [32].

[35] The total probability of all the many chain states cannot be normalized to unity [16].

[22] O. V. Kancheli, *Zh. Eksp. Teor. Fiz. Pisma Red.* **18**, 465 (1973) (English translation: *JETP Lett.* **18**, 274 (1973).
[23] E. S. Lehman, G. A. Winbow, *Phys. Rev.* **D10**, 2962 (1974).
[24] J. H. Weiss, unpublished.
[25] A. Schwimmer, *Nucl. Phys.* **B94**, 445 (1975); L. Caneschi, R. Jengo, A. Schwimmer, CERN TH-2104 (1976).
[26] A. Capella, J. Kaplan, *Phys. Lett.* **52B**, 448 (1974); A. Capella, J. TranTranh Van, J. Kaplan, *Nucl. Phys.* **B97**, 493 (1976).
[27] A. Capella, A. Kaidalov, CERN TH-2151 (1976).
[28] A. Capella, J. Kaplan, J. Tran Tranh Van, CERN TH-2083 (1975); N. S. Craigie, K. J. M. Moriarty, J. H. Tabor, CERN TH-2140 (1976).
[29] H. D. I. Abarbanel, J. Bartels, J. Bronzan, D. Sidhu, *Phys. Rev.* **D12**, 2798 (1975).
[30] J. B. Bronzan, *Phys. Rev.* **D10**, 746 (1974); J. L. Cardy, *Nucl. Phys.* **B75**, 413 (1974); A. Czechowski, *Phys. Lett.* **58B**, 85 (1975); H. D. I. Abarbanel, J. B. Bronzan, A. Schwimmer, R. L. Sugar, SLAC-PUB-1619, (1975) and Rutgers preprint (1976); D. Amati, M. Le Bellac, G. Marchesini, M. Ciafaloni, CERN TH-2152 (1976).
[31] M. S. Dubovikov, K. A. Ter-Martirosyan, Moscow 1976.
[32] N. N. Nikolaev, Report to Seminar on Particle-Nucleus Interactions, ICTP, Trieste, June 1976.
[33] Ya. Azimov, V. A. Khoze, E. M. Levin, M. G. Ryskin, *Nucl. Phys.* **B89**, 508 (1975).
[34] P. V. R. Murthy et al., *Nucl. Phys.* **B92**, 269 (1975).
[35] R. D. Field, G. C. Fox, *Nucl. Phys.* **B80**, 367 (1974).
[36] L. Caneschi, A. Schwimmer, *Nucl. Phys.* **B102**, 381 (1976).
[37] W. Busza et al., Paper submitted to the 17th Internat. Conf. on High-Energy Physics, London, June 1974.
[38] J. Kwieciński, L. Leśniak, K. Zalewski, *Nucl. Phys.* **B78**, 251 (1974).
[39] V. N. Gribov, Proc. of 8th Winter School of Physics, LNPI, Leningrad 1973.
[40] L. Bertocchi, S. Fubini, M. Tonin, *Nuovo Cimento* **25**, 626 (1962); D. Amati, A. Stanghellini, S. Fubini, *Nuovo Cimento* **26**, 6 (1962).
[41] T. Jaroszewicz, unpublished.